THEORETICAL SIMULATIONS OF UV-VIS AND UP SPECTRA FOR CONJUGATED SYSTEMS

A THESIS
SUBMITTED TO THE DEPARTMENT OF CHEMISTRY
AND THE INSTITUTE OF ENGINEERING AND SCIENCES
OF
BILKENT UNIVERSITY
IN PARTIAL FULFILLMENT OF THE REQUIREMENTS
FOR
THE DEGREE OF MASTER OF SCIENCE

By

Fahri Alkan

December 2009

I certify that I have read this thesis and that in my opinion it is fully adequate, in scope and in quality, as a thesis for the degree of Master of Science.

Assoc. Prof. Dr. Ulrike Salzner (Supervisor)

I certify that I have read this thesis and that in my opinion it is fully adequate, in scope and in quality, as a thesis for the degree of Master of Science.

Prof. Dr. Şefik Süzer

I certify that I have read this thesis and that in my opinion it is fully adequate, in scope and in quality, as a thesis for the degree of Master of Science.

Assist. Prof. Dr. Dönüş Tuncel

I certify that I have read this thesis and that in my opinion it is fully adequate, in scope and in quality, as a thesis for the degree of Master of Science.

Assist. Prof. Dr. Ceyhun Bulutay

I certify that I have read this thesis and that in my opinion it is fully adequate, in scope and in quality, as a thesis for the degree of Master of Science.

Assist. Prof. Dr. Daniele Toffoli

Approved for the Institute of Engineering and Sciences:

Prof. Dr. Mehmet B. Baray

Director of Institute of Engineering and Sciences

ABSTRACT

THEORETICAL SIMULATIONS OF UV-VIS AND UP SPECTRA FOR CONJUGATED SYSTEMS

Fahri Alkan

M.S. in Graduate Program of Chemistry

Supervisor: Assoc. Prof. Dr. Ulrike Salzner

December 2009

Due to their unique electro-optical properties, there has been a great deal of scientific interest in electronic structure of conjugated systems. In order to reveal the complete map of their electronic structure, several experimental investigations are done using UV-Vis and ultraviolet photoelectron spectroscopy (UPS). The experimental findings are usually interpreted by the results of quantum chemical calculations. In this study, we present the theoretical simulations of UV-Vis and UP spectra of conjugated systems by using density functional theory (DFT). In UV-Vis simulations, we investigated the excited states of oligothiophene anions and cations and almost identical UV spectra were obtained for these systems. This similarity in excitation energies are explained by the resemblance in energy levels and nature of excited states in anions and cations. In UPS simulations, the energy levels of

conjugated systems were calculated by using ΔSCF/TDDFT and DFT orbital eigenvalues. It is shown that there is a good agreement between ΔSCF/TDDFT and experiment, especially for the investigated oligomers. In contrast, DFT orbital energies are considerably lower than the experiment. However, spacing of energy levels is consistent with both experiment and ΔSCF/TDDFT.

Keywords: Conjugated systems, density functional theory (DFT), UV-Vis spectroscopy Ultraviolet photoelectron spectroscopy (UPS), thiophene, pyrrole, furan.

ÖZET

KONJUGE SİSTEMLERİN UV-VIS VE UPS SPEKTRUMLARININ TEORİK SİMULASYONLARI

Fahri Alkan

Yüksek Lisans Kimya bölümü

Tez Yöneticisi: Doç. Dr. Ulrike Salzner

Aralık 2009

Konjuge sistemlerin elektronik yapıları, gösterdikleri kendine özgü elektriksel ve optik özellikler sebebiyle bilimsel alanda oldukça fazla ilgi görmektedirler. Bu sistemlerin elektronik yapılarını ortaya çıkarmak amacıyla UV-Vis ve UPS spektroskopi tekniklerini kullanarak birçok deneysel çalışma yapılmıştır. Ayrıca deneysel sonuçlar kuantum kimyasal hesaplamalar kullanılarak açıklanmaya çalışılmıştır. Bu çalışmada da konjuge sistemlerin UV-Vis ve UPS spektrumları yoğunluk fonksiyonel teorisi kullanılarak (DFT) simüle edilmiştir. UV-Vis simülasyonları için tiyofen oligomerlerinin anyon ve katyonlarının uyarılma halleri incelenmiştir. Bu incelemeler sonucunda anyon ve katyonlar için çok benzer UV spektrumları elde edilmiştir. Bu sonuç sistemlerin enerji seviyeleri ve uyarılma hallerinin yapıları arasındaki benzerliklerle açıklanmıştır. UPS simülasyonlarında ise, konjuge sistemlerin enerji seviyeleri ΔSCF/TDDFT metodu ve DFT orbital enerjileri

kullanılarak hesaplanmış ve ΔSCF/TDDFT metodunun özellikle tiyofen ve furan oligomerleri için deneyle oldukça uyumlu olduğu gösterilmiştir. Buna karşın DFT orbital enerjilerinin deneysel sonuçlardan önemli derecede az olduğu bulunmuştur. Ancak enerji seviyeleri arasındaki farkların hem deney hem de ΔSCF/TDDFT metodu ile uyumlu olduğu gösterilmiştir.

Anahtar kelimeler: Konjuge sistemler, yoğunluk fonksiyonel teorisi (DFT), UV-Vis spektroskopisi morötesi foto elektron spektroskopisi(UPS) tiyofen, pirol, furan.

ACKNOWLEDGEMENT

I wish to express my gratitude to my advisor, Professor Ulrike Salzner for her great guidance and kindness during my studies.

I would like to thank Professor Şefik Süzer and Professor Ömer Dağ for their encouragements and valuable discussions.

I would like to acknowledge whole members of Chemistry Department at Bilkent University, my family and my friends for their moral support.

And finally, I would like to give my special thanks to Özlem Köylü whose patient love enabled me to complete this work.

Table of Contents

List of Figures

List of Tables

Chapter 1: Introduction

1.1 Motivation

Conjugated polymers have been an active area of research in both theoretical and experimental chemistry for more than 30 years. Those studies mainly focused on the semiconducting properties of these materials associated with the π orbitals delocalized on the polymer chain. In 1977, Alan J. Heeger, Alan MacDiarmid and Hideki Shirakawa reported very high conductivity for iodine doped polyacetylene [1] as they showed that its conductivity increased in 12 orders of magnitude. Their achievement has been rewarded with the Nobel Prize in Chemistry in 2000. Since then, conjugated polymers have been used in molecular based electronic and opto-electronic devices including light-emitting diodes, [2, 3] large area displays, [4] electrochromic structures and devices, [5] light harvesting materials [6, 7] and photovoltaic cells. [8] The use of conjugated polymers or oligomers instead of traditional semiconducting materials, such as silicon, is a very attractive field in material science due to their physical properties like electrical conductivity, electroluminescence, photoluminescence [9] and second and third order nonlinear optical activities, [10] and due to their polymeric properties like being less expensive, more disposable and easy to process. The unification of such mechanic and electronic aspects of conjugated polymers will enable them to be used as next generation electro-optical devices. Some of the common conjugated polymers are

polyacetylene, polypyrrole, polythiophene, polyfuran, polyaniline and poly(para-phenylenevinylene). These polymers have been studied extensively in order to understand their electronic and optical properties. Additionally, efforts are going on to synthesize new materials with specific properties by substituting functional groups or building co-polymers and new derivatives for furthering their usage. [11]

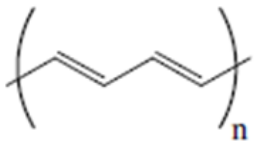		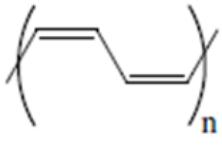
a) trans-polyacetylene		b) cis-polyacetylene
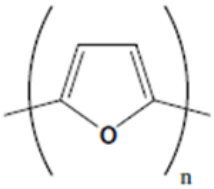		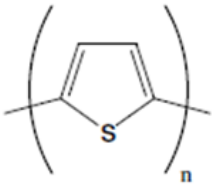
c) polyfuran		d) polythiophene
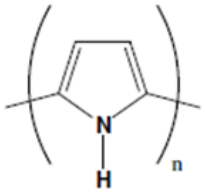		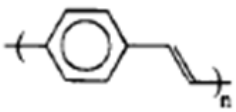
e) polypyrrole		f) poly-(p phenylenevinylen)

Table 1.1 Some of the common conjugated polymers

Physical properties of conjugated polymers

1.2.1 Polyacetylene

Polyacetylene is the simplest conjugated polymer built by $(CH)_n$ units with alternating double and single bonds. The neutral polyacetylene films are organic semiconductors with large band gap. However, upon p and n type doping they become highly conducting materials with conductivities as high as 1.5 x 10^5 S/cm upon p and n type doping. [12, 13] They form quasi-one dimensional structures because of the covalent bonding within chains and weak van der Waals interactions between the chains. Polyacetylene can be either in cis or trans conformation with trans being the thermodynamically stable one. [14] It is also reported that the trans conformation has a higher conductivity than its cis counterpart at room temperature. [1]

1.2.2 Polyheterocycles (Polythiophene, Polypyrrole and Polyfuran)

Polyheterocycles consisting of $(C_4H_4X)_n$ units with X=S, N and O for the systems will be the focus of our study. Their structure is analogous to the cis conformation of polyacetylene with the addition of heteroatom which stabilizes the system. [15] The conductivity of polypyrrole varies between 10^{-10} and 100 S/cm in insulating and conducting(doped) states. [16] In contrast, polythiophene has a room temperature conductivity of 50-100 S/cm. [14] However, some of the substituted polythiophene derivatives have conductivities above 1000 S/cm. [17] For both polyheterocycles, doping is associated with a color change and shift in the absorption energies. [18] Polyfuran is the least studied polyheterocycle among these three

because of the experimental difficulties in its synthesis and doping due to its high oxidation potential. [19] It is also reported that this difficulty can be overcome by changing the experimental conditions. [20, 21] The conductivities of polyfuran are ranging from 10^{-6} to 80 S/cm whereas the undoped form has a conductivity of 10^{-11} S/cm. The broad range of conductivities in the doped states is associated with the experimental conditions and different dopants. [19]

1.3 Conjugated oligomers

Conjugated oligomers are built from limited number of monomer units and they are intermediate between polymers and monomers in terms of their size. These materials have been investigated for their physical properties and emerge as a field of their own. However, most studies are focused on using conjugated oligomers as model compounds for corresponding polymeric systems by extrapolation of a certain property with increasing chain length. [22, 23] There are several advantages of this approach. The conjugated oligomers are easier to work on as they are more soluble than polymers. In addition, better resolution in spectroscopic studies could be achieved with well-defined monodisperse oligomers. [22] The oligomer approach is also preferable in theoretical studies because of the finite size of these systems.

Another important issue in modeling conjugated polymers by using oligomers is effective conjugation length. Due to distortions in the planar structure of conjugated backbone, π overlap could be in a limited length instead of a continuous network along the chain. Therefore, conjugation shows a convergence for long polymers. Several investigations have been done by employing oligomers in order to determine the effective conjugation length in polymers. [24-26]

1.4 Electronic structure of conjugated systems

1.4.1 Band structure of conjugated polymers

In contrast to the σ-bonded polymers such as polyethylene, conjugated systems have delocalized π network formed by the p_z orbitals of the sp^2 hybridized C atoms. This network of π electrons along the chain is the main factor for the electronic structure of conjugated systems. In a single monomer, atomic orbitals of C atoms and heteroatom form molecular orbitals which lead to discrete energy levels. As the chain gets longer, discrete energy levels of the single units interact and eventually form band structures and band gaps for polymers. Figure 1.1 visualizes such interactions in a schematic manner. In such conjugate systems, π states form the frontier molecular orbitals with a π band gap, which is relatively low (1-4eV) compared to band gap of σ systems. [27] The semiconducting character and low energy electronic excitations are the results of this π band gap.

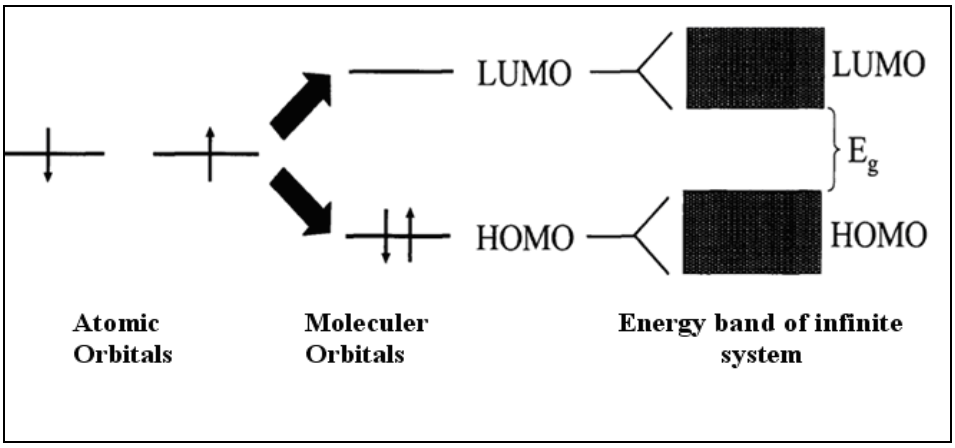

Figure 1.1: Formation of band structure from molecular orbitals in a qualitative picture

Due to Peierls distortion, carbon-carbon bonds are not equal in conjugated systems. This alternation in the bond lengths leads to energy gaps in the band structure, while highest occupied molecular orbital (HOMO) and lowest unoccupied molecular (LUMO) orbital would be degenerate in an infinite polyacetylene chain if carbon-carbon bonds were equal. In such a system, there would be no band gap and material would have a metallic character. However, Peierls distortion breaks the symmetry of the molecule which results in an energy difference between HOMO and LUMO levels.

1.4.2 Valence shell electronic structure of heterocyclic monomers

The outer valence shell of the conjugated monomers, oligomers and polymers has been studied extensively both theoretically and experimentally in order to understand the electronic structure of these molecules. The purpose of this section is to review the electronic structure of five-membered heterocycles; thiophene, furan and pyrrole.

The symmetry point groups of these systems are $C_{2v.}$ Four p-electrons from the carbons and two electrons from the lone pair of the heterocyclic atom (S, N and O) form the three occupied π molecular orbitals. The molecular orbital sequences in the electronic structure of these systems are investigated using photoelectron spectroscopy [28-30] and energy loss spectroscopy. [31, 32] Energy levels are assigned by the measurements done on the angular distribution of the photo-ionized electron and combined experimental and theoretical investigations. Table 1.2 shows the conclusions derived from these studies.

In all three molecules, two outer most energy levels arise from π molecular orbitals. In contrast, π3 levels interchange as the heteroatom changes in these cyclic systems. It is also reported that the assignment of the deep lying π3 orbital is somewhat difficult and subject of a debate. [33]

Thiophene	**Pyrrole**	**Furan**
$1a_2(\pi1)$	$1a_2(\pi1)$	$1a_2(\pi1)$
$2b_1(\pi2)$	$2b_1(\pi2)$	$2b_1(\pi2)$
$9a_1$	$1b_1(\pi3)$	$9a_1$
$1b_1(\pi3)$	$9a_1$	$8a_1$
$6b_2$	$6b_2$	$6b_2$
$8a_1$	$5b_2$	$5b_2$
$5b_2$	$8a_1$	$1b_1(\pi3)$
$7a_1$	$7a_1$	$7a_1$
$4b_2$	$4b_2$	$6a_1$
$6a_1$	$6a_1$	$4b_2$
$5a_1$	$3b_2$	$3b_2$
$3b_2$	$5a_1$	$5a_1$
$4a_1$	$4a_1$	$4a_1$

Table 1.2 The molecular orbital sequence for the monomers thiophene, furan and pyrrole.

1.4.3 Charge carriers in conjugated systems

Conjugated polymers mainly have quasi-one dimensional geometric structures and each carbon atom is coordinated with three neighbors. Therefore, the charge carriers in these systems are associated with combined lattice and charge distortions which differ from the traditional semi-conductors where the charge carriers are free

electrons or holes in a more rigid crystal structure with four or six-fold coordination. [14]

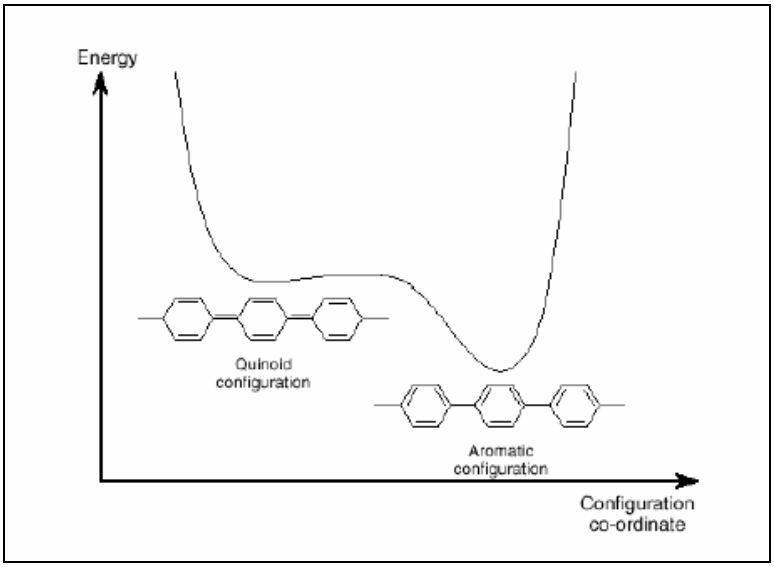

Figure 1.2: Potential energy diagram of aromatic and quinoid configurations of PPV.

There are mainly two different classes of coupled charge-lattice deformation regarding to degeneracy or non-degeneracy of the ground state of the conjugated system. These deformations can be triggered through optical absorption or doping. Polymers like trans-polyacetylene have a degenerate ground state and are susceptible to a defect which results in formation of the charge bearing species called as “soliton”. [34, 35] In contrast to trans-polyacetylene, polymers such as polythiophene or poly(para-phenylene) (PPV) have non-degenerate ground states meaning that the energy of the system alters upon the interchange of single and double bonds in the system. A qualitative potential energy diagram for these different configurations is shown in Figure 1.2. This interchange disturbs the aromaticity of the structure and forms the energetically less favorable quinoid structure. Due to non-degenerate ground state,

the deformations in such systems form polarons, the coupling of electron and phonon in the lattice. Further perturbation of the system such as oxidation or reduction results in formation of the spinless and doubly charged bipolarons. Figure 1.3 shows the structure of a polaron and bipolaron in PPV.

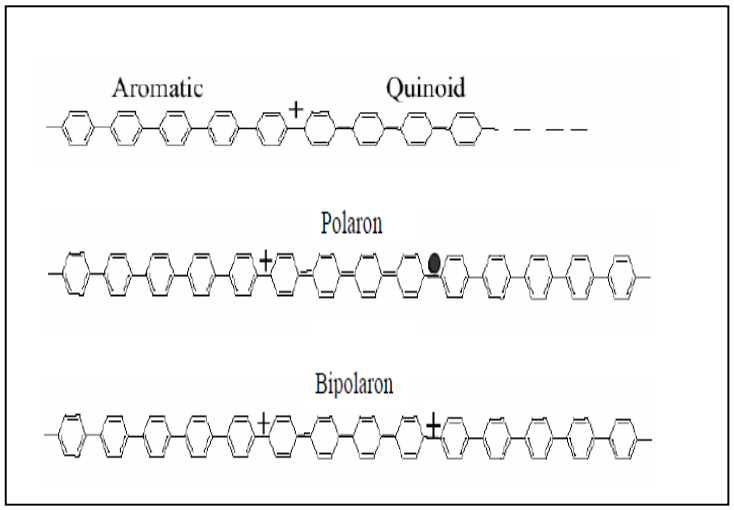

Figure 1.3: Formation of polaron and bipolaron defects in PPV

1.5 Ultraviolet absorption and photoelectron spectroscopy studies on conjugated systems. Spectroscopic fingerprints for electronic structure.

Several experimental techniques have been used to investigate the unique optical and electronic properties of the conjugated systems. However, ultraviolet absorption (UV) and ultraviolet photoelectron spectroscopy (UPS) are the most widely used experimental methods which are usually combined with theoretical predictions to understand the intrinsic electronic structure of such systems.

1.5.1 UV-Vis studies on conjugated systems

Experimental studies using UV spectroscopy are focused on recording the changes in the spectra upon doping of the conjugated system since they can reveal the fingerprints of the forming energy states during the charge transfer between dopant and the π-system.

Undoped trans-polyacetylene gives rise to a strong absorption with λ_{max} at 1.9 eV. This strong absorption is assigned to the π-π transition from the valence band to the conduction band. [14, 36] Upon doping, there appears a new and broad transition at near-IR regime. The interesting feature of this transition is that the energy of the transition does not depend on the type of the dopant and whether the doping is n-type or p-type. [37]

Chung et al. have investigated the doping effect on the absorption spectra of the polythiophene in a similar manner to trans-polyacetylene. [18] Undoped polythiophene shows a strong absorption with a λ_{max} at 2.7eV which shifts to higher energies and decreases in intensity as the dopant concentration increases. This absorption is believed to be the characteristic π-π transition from valence band to the conduction band. Additionally, there are two new features observed in the spectra at the IR regime with increasing doping level. These new two peaks merge into a very broad peak at very high dopant concentrations. Similar investigations have been conducted on polypyrrole as well. The UV-vis spectrum of the neutral polymer shows the π-π transition with a λ_{max} around 3.2eV. [38] This absorption shifts to higher energies and loses oscillator strength with increasing doping level like for polythiophene. However, reported UV absorption data show two or three new peaks upon doping with different dopants. [39, 40]

1.5.2 Polaron-bipolaron model

. The polaron-bipolaron model was developed by using the Su-Schrieffer-Heeger (SSH) Hamiltonian [34, 41] in order to rationalize the afore-mentioned spectral changes upon doping of conjugated systems. In this model, polaron and bipolaron deformations which form during doping process are associated with two new energy levels in the otherwise forbidden energy gap. [42-44] These new states are believed to give rise to three intra-band gap transitions when polarons form in the lattice. In contrast, the bipolarons are associated with two intra-band gap transitions. The new energy levels and the intra-band gap transitions in the polaron-bipolaron picture are shown in Figure 1.4. The observed high and low electron spin resonance (ESR) signals during the doping process are considered as evidence for the formation of polarons and bipolarons respectively in such systems since a polaron gives rise to an unpaired spin in the electronic structure whereas a spinless pair forms in the bipolaron case. [14, 45-47]

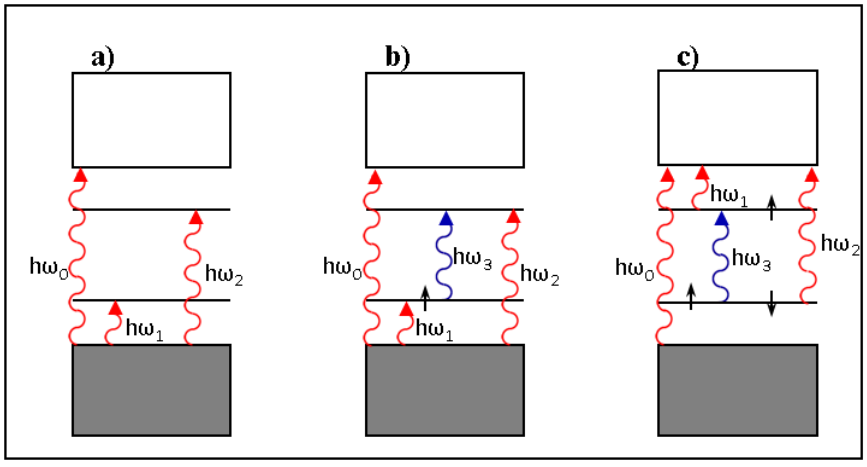

Figure 1.4: Optical excitations predicted for **a)** positively charged bipolaron and **b)** positively charged polaron. Note that there is an additional transition due to occupancy of lower level at mid-gap

Polarons and bipolarons are believed to be self-localized on the chain due to the competition between the favorable aromatic form and the more energetic quinoid form. For polypyrrole, localization of polarons was found to be over four rings at SSH level of theory. [48] Similar results were obtained for the polythiophene as well. [49] Additionally, the defect size of n-doped and p-doped systems were compared in the literature and it was found that while semi-empirical SCF methods yield smaller defect for anions, [50] ab-initio calculations predict indistinguishable geometries. [51]

In Figure 1.4, it is seen that the two energy levels in the gap are symmetrically placed. For polythiophene, this is rationalized by small interaction of S atom with the conjugated backbone. [52] Due to this symmetry, similar UV spectra are expected for p-doped or n-doped polythiophene (Figure 1.4b and 1.4c) at the Hückel [52] or SSH level of theories [34, 41] since the electron interactions are not considered explicitly and addition of electrons does not alter the symmetric placement of intra-gap states significantly. This electron-hole symmetry in the polaron-bipolaron model is confirmed experimentally for didodecylsexithiophene. [53]

The fact that polythiophene shows only two absorptions at low doping levels and one at high doping level, contradicts predictions of the polaron-bipolaron model. Moreover, doping experiments on the oligomers of thiophene indicates that the UV spectra of the cations show two absorptions and dications show only one [54-56]. Theoretical simulations of the UV spectra done on the oligothiophenes at the ab-inito level [57, 58] and with density functional theory (DFT) [59] also confirm the existence of two transitions for the cations. In contrast to the polaron-bipolaron model which predicts self-localized geometry defects as the underlying cause for the sub-band transitions, DFT excitation energies for thiophene cations are in good agreement with experiment with a delocalized geometry. [59] Additionally, energy levels and nature of excited states for the cations of thiophene and pyrrole oligomers

predicted at DFT level [59, 60] are very different when compared to polaron picture shown in Figure 1.3b. Therefore, there is experimental and theoretical evidence in the literature that shows that the polaron-bipolaron model does not fully explain the spectral changes in conjugated systems upon doping.

1.5.3 UPS studies on conjugated systems

UPS is another important tool for investigating the electronic structure of the conjugated systems because states of neutral species and new states created upon doping can be directly observed. The principle of this technique is to ionize the molecule by a quantum of radiation $h\upsilon$ and then measure the kinetic energy of the released photoelectrons. These quantities are related by the Einstein's famous relation:

$$T_n = h\upsilon - (I_n + E_{vib} + E_{rot}) \qquad \textbf{Eq. 1.1}$$

In this equation, I_n is the ionization potential of the molecule, T_n is the kinetic energy of the electron and E_{vib} and E_{rot} are vibrational and rotational energies of the remaining ion after photo-ionization. Rotational energies are quite small when compared to other terms of the equation and so can be neglected. Therefore the energy analysis of the photoelectrons yields the information about vertical and adiabatic ionization energies and the energy of cationic state. Additionally, vibronic structure may be revealed if enough resolution is obtained in the spectrum.

For the intrinsic electronic structural studies, UPS is mainly employed to record the valence electron spectra of the conjugated systems. In a similar manner to UV studies described in previous section, the UPS spectra of the neutral systems are compared to doped systems to observe the modifications and doping-induced

electronic states. [61-65] However, unlike UV spectroscopy, these states are only detectable in terms of UPS when they are occupied which is the case in n-doped systems. Such investigations are carried out on both conjugated polymers [61-63] and oligomers. [64, 65] Additionally, oligomers with different number of units are investigated to record the π band evolution and modifications of the electronic structure depending on conjugation lengths. [66-68] Recently, angle resolved techniques are applied to the heterocyclic monomers in order to assign the bands and reveal the complete valence electronic structure. [33, 69-71]

1.5.4 Koopmans's theorem and theoretical modeling of UPS

For a better understanding of the valence electronic structure of conjugated systems, UPS data have been usually combined with the theoretical predictions from quantum chemical calculations in many previous studies. At this step, Koopmans's theorem [72] builds a general basis for interpretation of the experimental spectra. Koopmans's theorem is mathematically exact at the Hartree-Fock level and states that in an N electron system, the ionization potential to produce an N-1 electron system is equal to the negative of the energy of the molecular orbital from which the electron is removed. Despite the popularity of using orbital eigenvalues instead of cationic states in modeling the experimental spectra, Koopmans's theorem suffers from two main errors; firstly, the electronic relaxations occurring upon the change in number of electrons in the system are neglected. It is reported that the photo-emitted electron typically leaves the molecule within about 10^{-14} to 10^{-16} sec. whereas electronic relaxations occur within 10^{-16} sec. [73] Therefore, electronic relaxations are included in the experimental data but not in the theory. Secondly, as Koopmans's

theorem is exact at the Hartree-Fock level of theory, electron correlation effects are missing from the start.

In order to simulate the appearance of experimental spectra and compare the results of theoretical predictions with experiment, either orbital eigenvalues or cationic states (see below) are convoluted by Gaussian or Lorentzian type functions. One photon transition rates in light-matter interactions are given by Fermi's golden rule:

$$R_{if} = \frac{\pi}{2}\Omega_0^2\,\delta(\omega - \omega_0) \qquad \textbf{Eq. 1.2}$$

In this equation, Ω_0 is the Rabi frequency which gives the strength of the coupling between electromagnetic field and transition dipole. Due to the presence of the delta function in the expression, the rate is zero for all frequencies ω except when it is resonant to the frequency of initial and final state ω_0. However, this is not the case in the experiment since the excitations never take place between two isolated states as vibrational and translational effects or intermolecular interactions are present in the experiment. Therefore, a more realistic picture can be achieved when the delta function is replaced by Lorentzian or Gaussian type functions. The latter is more popular for modeling of UPS.

$$L(\omega-\omega_0) = \frac{2}{\pi}\frac{\lambda}{(\omega-\omega_0)^2+\lambda^2} \qquad \textbf{Eq. 1.3}$$

Equation 1.3 represents the Lorentzian type broadening of the discrete orbital eigenvalues. Here λ is full width at half maximum (FWHM), a parameter that describes the resolution of theoretical spectra. Figure 1.5 shows the theoretical simulation of UPS by convoluting the discrete energy levels.

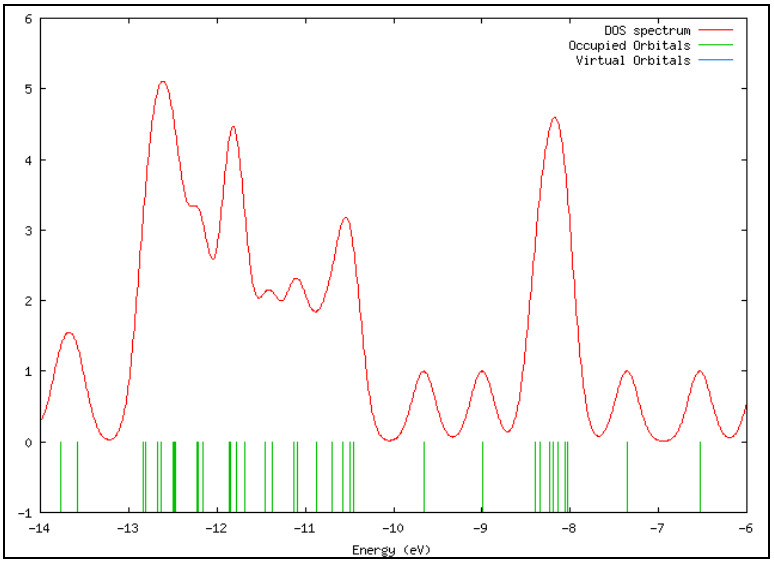

Figure 1.5: Theoretical modeling of the UPS. Discrete energy levels (bottom) are convoluted by 0.3 eV (FWHM).

Further consideration of the inter-molecular interactions is needed when theoretical results are compared with spectra of solid state samples. The remaining hole after photo-ionization is further stabilized in the condensed phase since it can be polarized by surrounding molecules in the crystal structure. [74] Sato et al. [75] measured the polarization energy for several organic molecules and a variation between 0.9 eV - 3.0 eV was observed. Aromatic hydrocarbons with planar structures have a common value of 1.7 eV which is independent of their size and crystal structures. The energy differences between orbital eigenvalues and ionization potentials of solids are rationalized by this polarization energy in several theoretical studies. [65, 76, 77]

1.5.5 Break-down of orbital picture: Shake-up satellites

According to the frozen orbital approximation in the Koopmans's theorem, the ionization energy is equal to the negative of orbital energies and all the ionization intensity belongs to the one electron transition from this orbital. However, correlation effects upon ionization of an electron can lead to multi-electron processes called shake-up satellites. The shake-up state can steal intensity from the main line that is described by one-electron ionization. An illustration of the one electron and multi-electron processes including photo-ionization and a HOMO→LUMO excitation that leads to a shake-up structure is shown in figure 1.6.

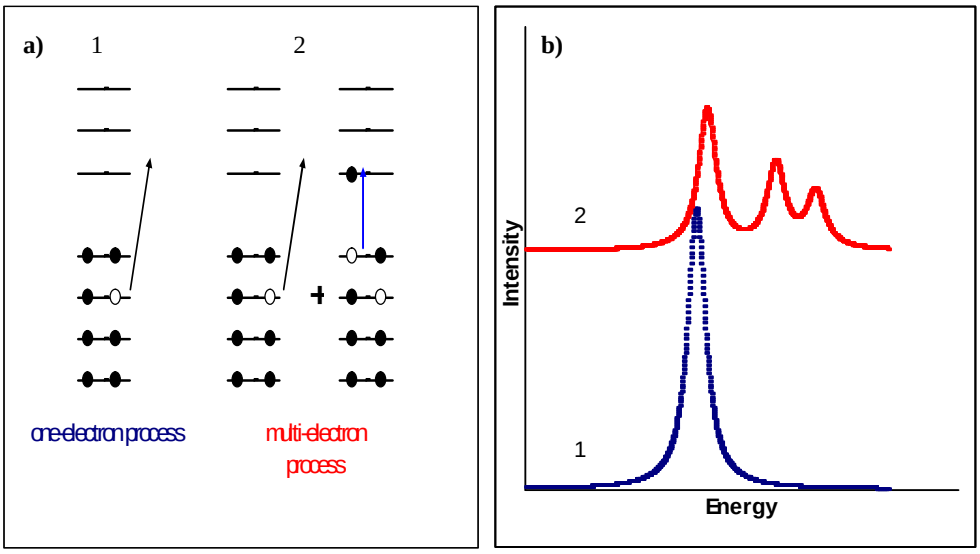

Figure 1.6: a) An illustration of one-electron and multi-electron photo-ionization b) appearance of the shake-up satellites in the spectra

Satellite structures in the valence region of conjugated systems are investigated experimentally by UPS using synchrotron radiation. [33, 78, 79] However, a difficulty arises with assignment of satellite bands in the spectra as they can be

confused with vibrational progression [80] since both give a broadening effect to the band. Electron momentum spectroscopy (EMS) is another useful technique in analyzing satellite structures. With this technique, one can extract the momentum profile of the ejected electron which enables the identification of the ionized orbital and the origin of satellite lines. EMS technique is applied to the monomers of heterocyclic conjugated systems [81-83] and significant break-down of orbital picture is found for the $1b_1(\pi)$ level in furan and pyrrole.

1.5.6 Previous theoretical investigations in the literature

Early theoretical investigations of UPS of conjugated systems started with the Hückel method for a limited number of hydrocarbons. [84, 85] This method could be applied to few molecules since new parameterizations are necessary for each type of atom in the system. These studies were followed by other calculations using the semi-empirical self-consistent-field (SCF) Pariser-Parr-Pople (PPP) method. [86] Different versions of the original method were used to predict the π orbital energies with good results for relatively small conjugated systems. [87-89] The semi-empirical treatment of similar systems continued with Hartree-Fock based semi-empirical methodologies. Several investigations have been done by Duke and his coworkers using spectroscopically parameterized complete neglect of differential orbitals (CNDO/S3) technique. [90-96] Calculations were carried out by using six different parameters for each atom. This method is proved to work better than simple ab-initio methods for some systems. However, the negative HOMO energy extracted from theoretical calculations is matched with experimental first ionization potential (IP) and higher energy levels are exposed to a linear shift with this matching value.

[91, 95] Additionally, the method fails to describe the inner-valence states as more complicated relaxations are present, which cannot be described by the empirical parameters in this method.

Another important approach that is widely used by Bredas and Salaneck in order to describe the electronic structure of conjugated systems is the valence electron Hamiltonian (VEH). This method is mainly a nonempirical pseudopotential technique with the use of an effective Fock Hamiltonian. However, atomic potentials in the Hamiltonian are parameterized using model molecules to produce Hartree-Fock results with double zeta basis sets. [98, 99] The VEH formalism has been applied to both conjugated polymers [99-101] and oligomers [65, 76, 77] and for the interpretation of newly formed gap states (polarons and bipolarons) upon doping of these systems. [64, 65] It should be noted that calculated energy levels are contracted systematically as the method reproduces too wide band widths. Moreover, the energy levels are exposed to a linear shift of 3.3 eV in order to account for the solid state polarization effects. This value contradicts with previous investigation of Sato et al. [75] as this solid state effect was shown to be 1.7 eV for aromatic hydrocarbons experimentally. We also report that both gas phase and solid state data is available for oligothiophenes [66, 67] and the differences are in the range of 0.8-1.2 eV. Therefore, the shift is mainly an empirical correction to adjust the results to match experiment. The atomic potentials in the Hamiltonian have been parameterized for only a limited number of atoms (C, H, S, N, Si and O) [76] so that counter ions and their interactions which are present in doping experiments cannot be modeled explicitly with VEH calculations. Additionally, geometry optimizations cannot be done at the VEH level. Therefore, the geometries of the investigated systems are obtained with semi-empirical methods.

Along with the CNDO/S3 and VEH methods, several other theoretical approaches exist in the literature to model valence electron spectra of conjugated systems. These approaches include semi-empirical methods; Austin model 1 (AM1) and intermediate neglect of differential orbital (INDO) [76] and modified neglect of differential orbitals (MNDO). [67, 68] The first principle symmetry adapted configuration interaction (SAC-CI) method is also applied to the conjugated systems and shown to be very accurate; however, it can be applied only to small systems (monomers). [102] Recently, the one electron Green's function approach with third order algebraic diagram construction (ADC(3)) is employed to some common conjugated monomers. [33, 103] In this theory, Hartree-Fock orbital energies are improved by self energy corrections that account for correlation effects upon ionization. This method provides accurate calculations for heterocyclic monomers (furan, thiophene and pyrrole). Additionally, satellite states can be obtained in this method. However, the computational complexity of self energy corrections is too demanding and the applicability of the method to larger system is an open question as there are no ADC(3) data available in the literature for the oligomers of the afore-mentioned heterocyclic systems.

1.5.7 The correlation between UV and UPS

There is a relation between UP spectra of neutral species and UV spectra of the corresponding cations as higher IPs of the neutral molecules produce excited states of the radical cations. [104] This close relation is shown in Figure 1.7 as the different transitions in parent molecule and the cation yield the same final state. Shida et al. [105] showed this correlation for different series of aromatic hydrocarbons and

amines by comparing ΔIP values (the energy difference of higher IPs relative to the first IP) and UV absorption data. This comparison yields very similar results for investigated systems. However, there are two important aspects of this methodology needs further consideration. The match between vertical ΔIP values and UV data can be done if there is no considerable change in geometric conformation of the cation upon ionization. It should also be noted that states that are present in the UPS might be unreachable through absorption if the transitions are optically forbidden

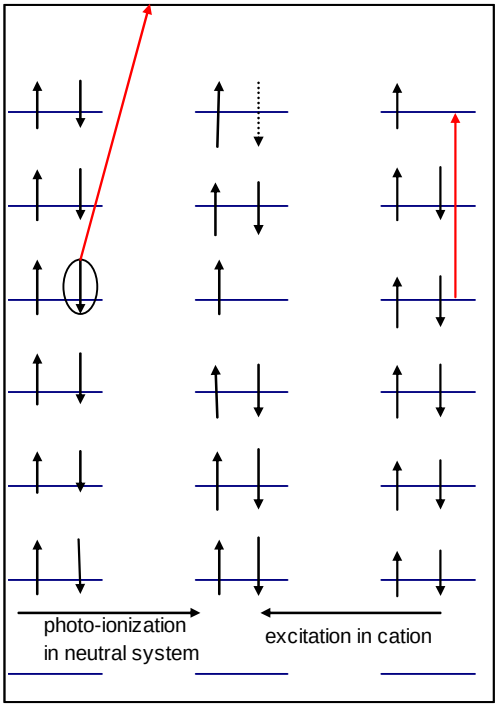

Figure 1.7: The correlation of photo-ionization and excitation in neutral and cationic systems.

1.6 The scope of this study

Since there are both experimental and theoretical contradictions with polaron-bipolaron model, the question arises if electron-hole symmetry can be confirmed in a more advanced theory where electron interactions are considered explicitly. Therefore, the first part of the present study is dedicated to address the question whether electron-hole symmetry is confirmed at the DFT level. To do that, we investigate geometries and excited states of thiophene oligomers for singly charged anions and the results are compared with the corresponding cation data obtained at the same level of theory. We use time dependent density functional theory (TDDFT) to calculate the excited states explicitly and to account for correlation effects which are missing in the polaron-bipolaron model.

In the second part of this study, we extended our discussion of excited states to the theoretical modeling of UPS in conjugated systems. We use the excited states of cations in order to simulate the UPS by using TDDFT. The main aim of this approach is to include electron relaxation and correlation effects which are missing in the Koopmans's theorem but are present in the experimental data. The rationalization of this methodology is made by using the correlation between excitation in cation and photo-ionization of parent molecule as shown in Figure 1.7. We also test the applicability of DFT orbital energies to predict the energy levels in conjugated systems. In this aspect, we compare the DFT results with previously mentioned excited state calculations and experiment.

Chapter 2: Theoretical background

Primary objective of the quantum chemistry is to reveal the electronic structure of atoms and molecules. To do this, we seek the solutions of the time-independent Schrödinger's equation which describes the quantum state of a system:

$$H\Psi = E\Psi \qquad \textbf{Eq. 2.1}$$

The equation is adapted to concentrate on electronic structure by Born-Oppenheimer approximation. This approximation takes note of the large mass difference between electron and nuclei. Therefore, the electronic and nuclear motion is separated and the nuclei are regarded as fixed in position. This procedure reduces the full Hamiltonian in equation 2.1 to electronic Hamiltonian. For an N electron atomic or molecular system, the electronic Hamiltonian in atomic units is given as:

$$H = -\sum_{i}^{N}\frac{1}{2}\nabla_i^2 - \sum_{i}^{N}\sum_{l}^{M}\frac{Z_l}{r_{il}} + \sum_{i}^{N}\sum_{j>i}^{N}\frac{1}{r_{ij}} \qquad \textbf{Eq. 2.2}$$

In the equation 2.2, the first summation describes the kinetic energy of the N electron system. The second term describes the potential energy between electrons and the nuclei. The last term takes account of the interaction between ith and jth electron in the system. This term distinguishes the Hamiltonian in equation 2.2 from hydrogen like systems and it is not possible to generate exact solutions for Schrödinger's equation due to this term. At this point, approximations are needed for further investigations of the multi-electronic systems. Several techniques and methodologies have been presented regarding to this problem. Better description of chemical

systems by using theory and development of new methodologies for quantum calculations are still active research areas for both chemistry and physics. It is the purpose of this chapter to review the basic formalisms of electronic structure theory.

2.1 Ab initio calculations

The term ab initio refers to “from the beginning” and comes from Latin. It indicates that the quantum calculation comes from first principles (such calculations are also referred as first principle calculations) and equation 2.1 is solved using only fundamental constants and atomic numbers. The model for the choice of wave function is crucial in this method and usually determines the accuracy. The simplest ab initio method is the Hartree-Fock (H.F.) formalism. The other popular quantum chemistry methods in this class (also known as post H.F. methods) are Moller-Plesset perturbation theory (MP_n), configuration interaction (CI) and coupled cluster (CC) theory. Ab initio calculations involve many integrals to evaluate and are computationally very expensive. Therefore, accurate calculations can be performed on relatively small molecules.

2.2 Semi-empirical methods

The second main approach in the pursuit of solving the multi-electronic Schrödinger’s equation is with the use of semi-empirical methods. The basic idea behind these methods is to simplify the Hamiltonian and reduce the number of integrals in quantum calculations by using adjustable parameters and values obtained from experimental data. The basic semi-empirical methods are Complete Neglect of

Differential Overlap (CNDO), Intermediate Neglect of Differential Overlap (INDO), Modified Neglect of Differential Overlap (MNDO), and Austin Model 1 (AM1). Accurate calculations may be obtained with this approach for larger molecules than with ab initio methods. However, applicability of a semi-empirical formalism is questionable when different atoms without suitable parameters are introduced into the system.

2.3 Density Functional Methods

Using electron density as a functional for the ground state energy is first shown by an early work of Thomas and Fermi. [106] However, this approach gained its popularity after the formal proof by Hohenberg and Kohn was given that *H* in equation 2.2 is a unique functional of the electron density. [107] Hence, the ground state energy and other electronic properties can be extracted from ground state electron density *p(r).* This was a revolutionary idea in the history of quantum chemistry since instead of dealing with complicated N electron wave functions; one can describe the system by one scalar function *p(r)* with three variables.

The formalism of the DFT was developed by Kohn and Sham after the formal proof was given. [108] The ground state energy as a function of density is given by equation 2.3.

$$E[p] = -\frac{1}{2}\sum_{i}^{N}\int \varphi_i(r_1)\nabla^2\varphi_i(r_1)dr_1 - \sum_{i}^{N}\int V(r_i)p(r_1)dr_1 + \frac{1}{2}\int \frac{p(r_1)p(r_2)}{r_{12}}dr_{12} + E_{xc}[p] \qquad \textbf{Eq. 2.3}$$

Here, the first term represents the kinetic energy of the N particle; second term represents the interaction of electron density with the external potential (nuclei) and

the third term shows the Coulomb repulsion of electrons in total density. All the exchange and correlation effects in the system are handled by the last term called exchange-correlation functional. However, the problem with this term is that the exact form of the functional is not known.

Several efforts have been made to predict the form of the exchange-correlation functional. Early approaches use the local density approximation (LDA) and local spin density approximation (LSDA). These studies are followed by gradient corrected density functionals and hybrid functionals. The popular exchange functionals are Becke 88 (B88) [109] and Perdew-Wang 86 (PW86) [110] and correlation functionals are Lee-Yang-Parr (LYP) [111] and Perdew 86 (P86). [112]

2.3.1 The meaning of DFT orbital energies and band gap problem

There is no equivalence of Koopmans's theorem in DFT, which would relate the Kohn-Sham orbital eigenvalues to the IPs. However, it was shown that the eigenvalue of the HOMO in DFT is equal to the negative of exact first IP if the exact exchange-correlation functionals is employed. [113, 114] In practice, this relation does not hold due to the insufficient cancellation of self-interaction with approximate functionals. Due to this error, DFT orbital energies are lower than experimental values by several eV. [115-117] However, this deviation from experiment is often the same for all valence orbitals in a given system.

Another fundamental problem in DFT is the underestimation of band gaps which is again the result of the self-interaction error in approximate functionals. [117] It is shown that the use of hybrid functionals with HF exchange could improve

the results for band gaps as the addition of exact exchange results in further cancellation of the self-interaction term. [118]

2.3.2 Time dependent density functional theory (TDDFT)

TDDFT extends the discussion of ground state in DFT formalism to time-dependent potentials and excited states. The formal foundation of the method starts with the proof of Runge and Gross which states that time-dependent wave function and hence all the physical observables can be determined by the knowledge of time-dependent density of a many-body system [119]. For valence excited states, TDDFT approaches to the accuracy of high level wave function methods with a low cost of computational time [120]. However, TDDFT could be problematic for neutral large π-systems as they suffer from the fast decrease of excitation energies [121] whereas the method performs better on the open-shell systems. [122]

2.4 $\Delta SCF_{(n)}$ methods

In contrast to the time dependent methods, excited states of a system can be calculated directly by a ground state method if the ground state calculation can be forced to yield higher energy solutions. This can be done by introducing symmetry constraints for the initial guess of the wave function given that the excited state belongs to a different irreducible representation of the point group of the system. This methodology is quite useful when one seeks the higher energies of cationic states in a UPS simulation. However, the method breaks down when the cationic state of interest belongs to the same symmetry as a lower energy solution. This

particular disadvantage of the method could be severe in a molecule with a low symmetry. Additionally, the method is computationally demanding since a different SCF calculation is needed for every excited state.

2.5 Methods used in this investigation

All calculations in this investigation are done with Gaussian 03, revision 02. [123] The geometry optimizations for the molecules investigated are done by employing DFT with Becke's three parameter hybrid functional and P86 correlation functional [111, 124] modified to have %30 H.F. exchange (B3P86-30%). [118] For the basis set, Stevens-Basch-Krauss pseudopotentials with polarized split valence basis sets (CEP-31G*) are used. [125, 126] The excited state calculations are done by employing TDDFT with same exchange-correlation functional and basis set.

For the UV spectra simulations, excited states of optimized oligothiophene anions with up to 19 rings are calculated. The geometries of anions are investigated in terms of defect size and compared with the cations. Additionally, the excitation energies of anions are compared with those of cations obtained at the same level of theory [59] in order to test if electron-hole symmetry is confirmed DFT calculations. For the UPS simulations, a new methodology will be established that is called ΔSCF/TDDFT. IP energies are calculated using three different techniques for comparison:

1. DFT orbital energies DFTϵ_n: negative of DFT orbital eigenvalues are used as IP energies in the system.

2. $\Delta SCF_{(n)}$: cationic states are calculated directly by applying symmetry constraints and the difference between the energy of the cationic state and the energy of the neutral system is used as IP energy.

3. ΔSCF/TDDFT: the first IP is computed by ΔSCF procedure, higher IP energies are calculated by adding excited state energies of the cation to ΔSCF value. The excited states with electron configurations dominated by nβ→(HOMO)β (shown in Figure 2.1) are taken as corresponding cationic states with ionization from nth level

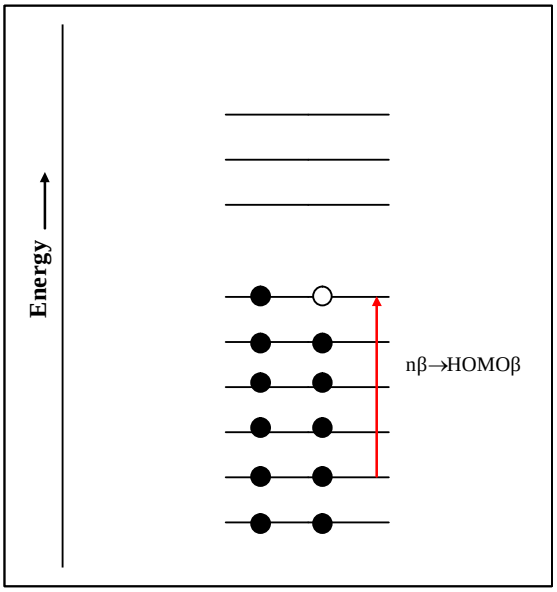

Figure 2.1: nβ→(HOMO)β transition in the cation.

Chapter 3: Results and discussion

3.1 UV spectra simulations for anions of thiophene oligomers by employing TDDFT

In order to simplify the nomenclature, electron configurations that contribute to excitations are designated in a similar manner to Pariser [127] notation. The visualization of this notation is shown in figure 3.1.

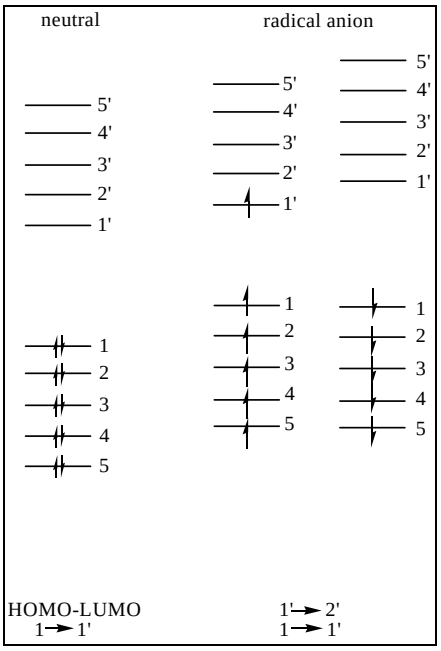

Figure 3.1: The notation to show electron configurations in excited states.

The HOMO level is numbered as 1 in the neutral system and the numbers increase as we move to deeper-lying orbitals. For the virtual orbitals, the LUMO level is designated as 1' and the numbers increase as we move to higher levels. The same nomenclature is used for anions as well. However, due to extra charge, there is an electron at 1' level.

3.1.1 Geometries

The comparison of the bond length changes in anion and cation of a thiophene oligomer with 19 rings (19T), with respect to the geometry of the neutral form is shown in Figure 3.2. It can be seen that bond length changes are quite similar except for the fact that the defect is slightly more localized in the case of anions. Additionally, overall variation from neutral geometry for anions is smaller than for the cations. In both cases, the defect is delocalized over the whole chain except for a few terminal units and the bond length changes are not large enough to convert single-double bond pattern. Therefore, we conclude that there is no transition of aromatic to quinoid structures for thiophene oligomers in the absence of counterions. In the presence of a counterion, the defect turns out to be more localized. The difference is shown in Figure 3.3 where the bond length changes in $13T^{-}$ and 13T-Na are compared. In 13T-Na, geometry distortion increases at the center of the chain where sodium is located and the interaction between chain and counterion is largest. In contrast, the terminal rings that include the first 12 carbon-carbon bonds almost remain unaltered. It should be noted that very similar results are obtained in the case of cations as well. [59] We also calculate the energy difference between the optimized anion and the bare anion in 13T-Na geometry by performing a single point

energy calculation. This difference is found to be 1.39 kcal/mol which implies that the geometry of the anion is very flexible and adjustable according to counterion position.

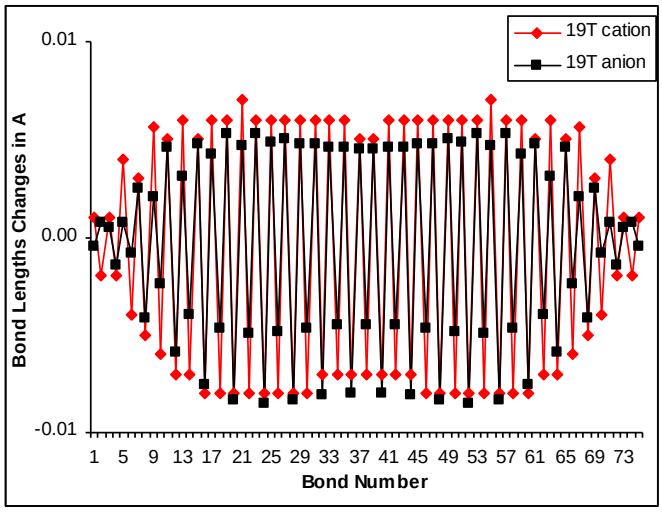

Figure 3.2: C-C bond length changes in $19T^-$ anion (black squares) and $19T^+$ cation (red diamonds) compared to neutral 19T.

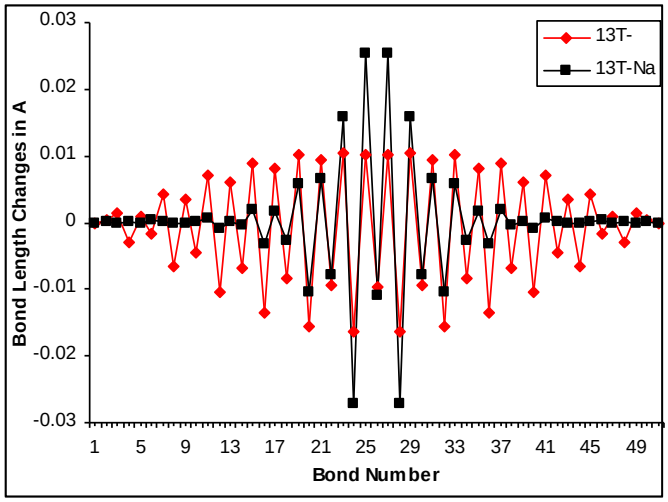

Figure 3.3: C-C bond length changes in $13T^-$ (red diamonds) anion and 13T-Na (black squares) compared to neutral 13T.

The main issue with of geometries of conducting polymers is the defect size upon doping. Although, pure DFT tends to overestimate the defect size, it is reported that B3P86-30% hybrid functional shows close agreement with MP2 geometries for polyene cations. [128] Furthermore, the problem of spin-contamination which occurs in polyene cations is not present for oligothiophene cations for B3P86-30% level of theory. [59] This is also true for the oligothiophene anions as the highest spin expectation value that we observe is 0.82 for $8T^-$.

3.1.2 Excited states of oligothiophene anions

In order to test how the presence of solvent and counterion affect the spectra of anions, 5T was optimized with the polarized continuum method (PCM) [129] in the presence of CH_2Cl_2 as solvent, with a sodium counterion. Figure 3.4 shows these results along with the excited states of bare $5T^-$ anion.

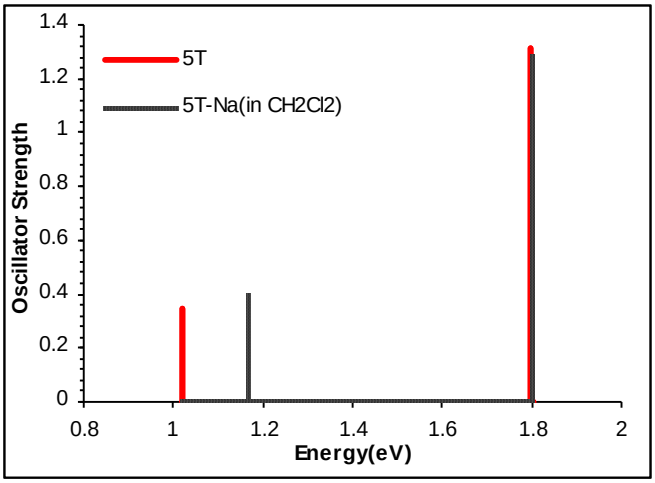

. **Figure 3.4:** Effect of counterion and solvent on the excitation energies and oscillator strengths for $5T^-$.

The first excitation energy increases 0.18 eV with a small gain in oscillator strength. The second excitation energies and their oscillator strengths are the same in both systems. For oligothiophene cations, it was reported that the simultaneous effects of solvent and counterion cancel partially since solvent alone leads to a small red shift to excitation energies while counterion leads to a blue one. [59] Therefore, the effects are very small on the spectra. Since this is also the case for the anions, we will consider gas phase calculation of excited states with bare ions for the rest of the discussion

Table 3.1 shows the comparison of excitation energies and oscillator strengths of cations and anions of thiophene oligomers. Experimental data extracted from UV spectra are available for didodecylsexithiophene cations and anions [53] and also included. The agreement between experimental and theoretical data is very good as the difference varies between 0.06 eV to 0.17 eV. Compared to cations, anions absorb at slightly lower energy, by up to 0.15 eV for E1 and 0.02 eV for E2. This is also confirmed in our calculations. The largest differences between excitation energies of cations and anions are 0.1 eV and 0.06 eV for E1 and E2 respectively and reported for 5T. As we get to the longer chain lengths this difference tends to decrease and perfect electron-hole symmetry is predicted. Stick spectra for $5T^{-}$ through $8T^{-}$ are plotted in Figure 3.5 and for $9T^{-}$ through $19T^{-}$ in Figure 3.6. For $5T^{-}$ to $8T^{-}$, there are two excited states with significant oscillator strengths. The first excited state arises from 1'$\rightarrow$ 2' electronic transition and shifts to lower energies with a gain in oscillator strength as the chain length increases. The second excited state is dominated by the 1$\rightarrow$ 1' transition and follows the same trend up to $9T^{-}$. However, starting from $9T^{-}$, intensity of this transition decreases with increasing chain length and a new transition occurs at 2.44 eV with significant oscillator

strength. The intensity of this transition increases considerably as we move to longer chain lengths. The inverse relation in the intensities of E2 and E3 is due to the fact that both these transitions are dominated by $1\rightarrow 1'$ and $2\rightarrow 1'$ electronic configurations.

Cations	E1	E2	E3
$5T^+$	1.12(0.33)	1.86(1.53)	-
$6T^+$	0.96(0.53)	1.68(1.70)	-
Exp.[a]	0.87	1.60	
$8T^+$	0.74(1.00)	1.45(1.75)	2.56(0.16)
$9T^+$	0.65(1.23)	1.37(1.67)	2.42(0.38)
$12T^+$	0.46(1.76)	1.21(1.21)	2.14(1.38)
$13T^+$	0.41(1.86)	1.17(1.07)	2.08(1.90)
$16T^+$	0.31(1.99)	1.09(0.71)	2.00(3.54)
$19T^+$	0.24(1.99)	1.05(0.50)	1.95(5.12)
Anions	E1	E2	E3
$5T^-$	1.02(0.35)	1.80(1.32)	-
$6T^-$	0.89(0.52)	1.64(1.50)	-
	0.72	1.58	
$8T^-$	0.69(0.91)	1.43(1.65)	-
$9T^-$	0.61(1.11)	1.36(1.54)	2.44(0.30)
$12T^-$	0.44(1.57)	1.22(1.27)	2.15(1.11)
$13T^-$	0.40(1.67)	1.19(1.14)	2.10(1.56)
$16T^-$	0.30(1.81)	1.11(0.82)	2.01(3.24)
$19T^-$	0.24(1.83)	1.07(0.60)	1.96(4.82)

Table 3.1 Energies and oscillator strengths (in parenthesis) of the three transitions for 5T-19T anions and cations.

a) Ref. 53

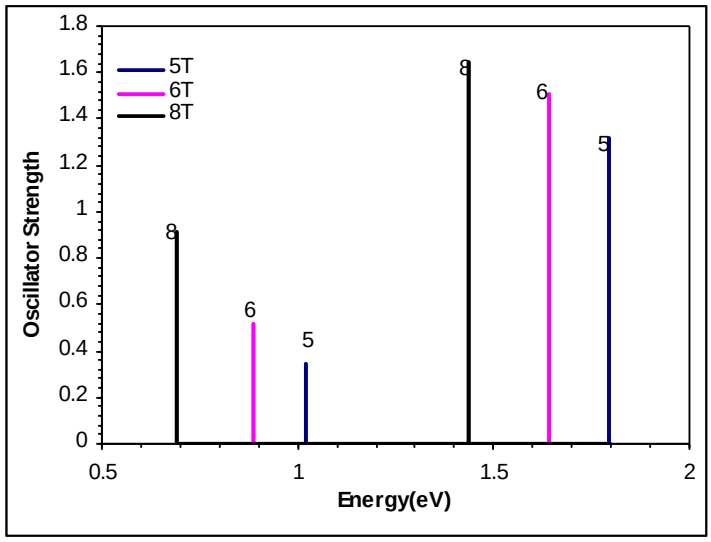

Figure 3.5: Stick spectra for 5T, 6T and 8T anions

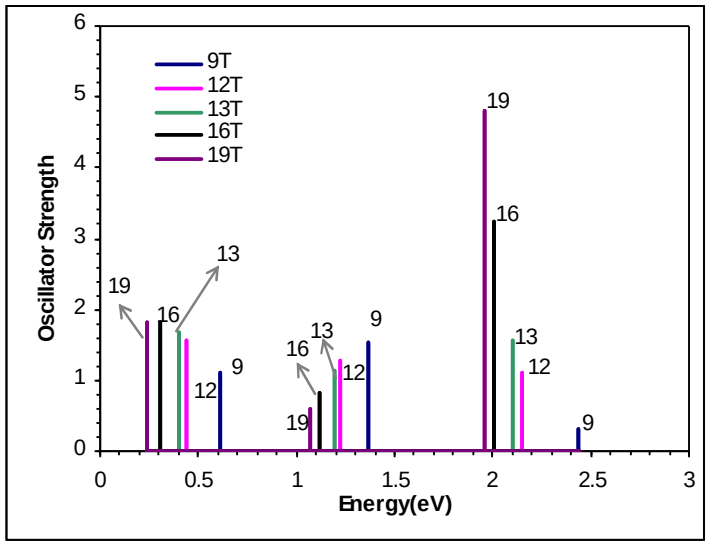

Figure 3.6: Stick spectra for 9T, 12T, 13T, 16T and 19T anions.

3.1.3 Dependence of absorption energies and oscillator strength on chain lengths

The changes in the absorption energies and oscillator strengths for different chain lengths of oligothiophene anions are summarized in Figures 3.7 and 3.8. For the three excited states, absorption energies decrease with chain length in a convergent behavior. However, the level of convergence is somewhat more obvious for second and third excitation energies. The oscillator strength of the first excited state shows a linear increase up to $12T^-$ and slowly converges in long chain limit. The oscillator strength of the second and third excited state is somehow correlated since the second excitation starts to lose oscillator strength as soon as third excitation shows up in the spectra. On the other hand, the third excitation starts as a weak feature at $9T^-$ in the spectra and becomes the dominant peak for $16T^-$ and $19T^-$. Therefore, we conclude that spectral changes should occur for n/p-type doping in the long chain length.

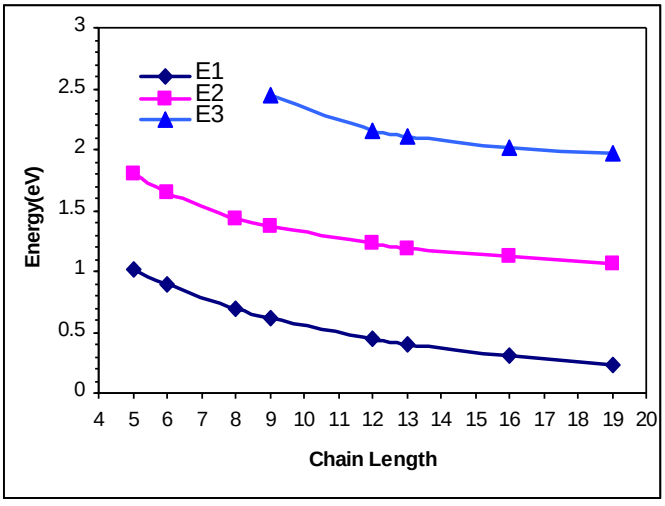

Figure 3.7: Excitation energy vs. chain lengths of the three sub-band absorptions of 5T-19T anions.

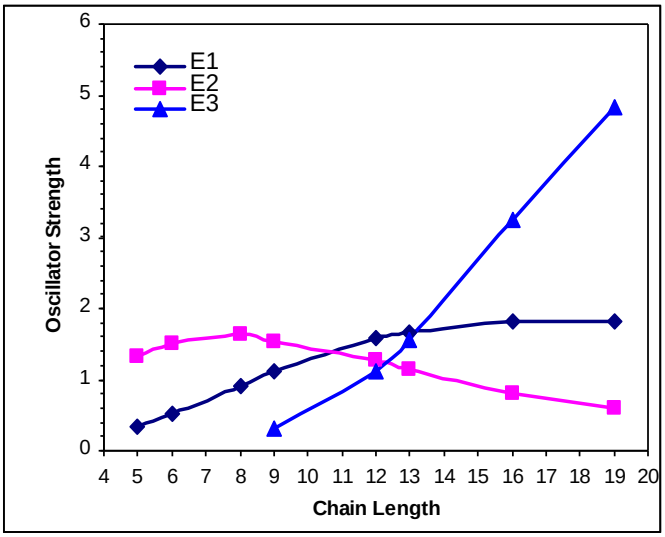

Figure 3.8: Oscillator strength vs. chain lengths of the three sub-band absorptions of 5T-19T anions

3.1.4 Electronic transitions and orbital energies

As shown in table 3.1, there is almost perfect electron-hole symmetry between the anions and cations of oligothiophenes. In order to make a deeper analysis on this matter, we compare the energy levels of $12T^{-}$ and $12T^{+}$ obtained with B3P86-30% level of theory. This comparison is displayed in Figure 3.9. It can be seen that there is only one intra-gap level predicted. In the case of anion, the level where the electron is added moves down in energy whereas in the cation, the level where the electron is removed moves up in energy. This picture contradicts with the polaron model (Figure 1.3) where two symmetric intra-band states are predicted. However, the polaron model is developed with the use of SSH Hamiltonian, [34-41] an extended Huckel formalism, which does not account the electron interactions explicitly. As a result, the position of intra-gap states does not alter significantly if extra electrons are added to energy levels. In contrast, number of electrons alters the

levels significantly at the B3P86-30% TDDFT level of theory. The only analogy with the polaron model is the symmetry of the difference of the anion level from the conduction band and the difference of cation level from valence band. (0.62 eV and 0.60 eV respectively)

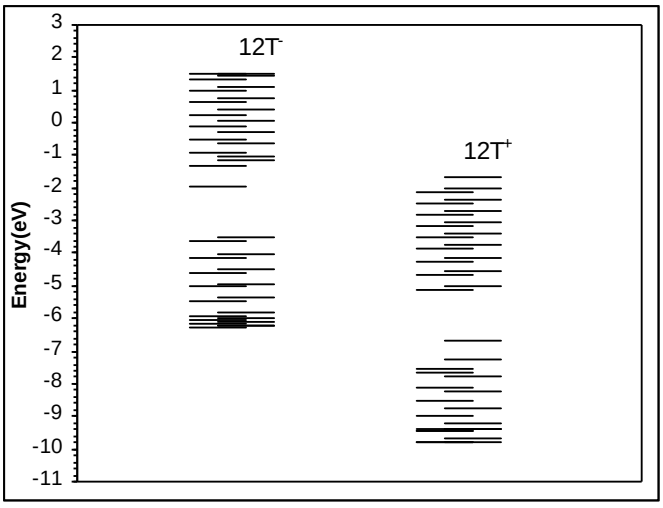

Figure 3.9: Orbital energies of $12T^{-}$ (left) and $12T^{+}$ (right).

Figures 3.10 and 3.11 display the orbital energy levels along with corresponding electronic transitions in the excited states for $12T^{-}$ and $12T^{+}$. We see that energies of excitations, oscillator strengths, the main electronic configurations and oscillator strengths are very similar for anion and cation. Additionally, there is mirror image symmetry between energy levels and electron configurations that contributes to the excited states. The first excited state is dominated by one electron transitions which are $2\rightarrow1$ and $1\rightarrow1'$ in cation and anion respectively. Therefore, the similar energy and oscillator strength for this excited state can be explained by the fore-mentioned symmetry of anion and cation level in the intra-gap. On the other hand, the second and third excited state has multi-configurational character.

However, the energies and oscillator strengths of the excited states are very similar in anion and cation due to the mirror symmetry of energy levels, electronic configurations and the coefficients of these electronic configurations.

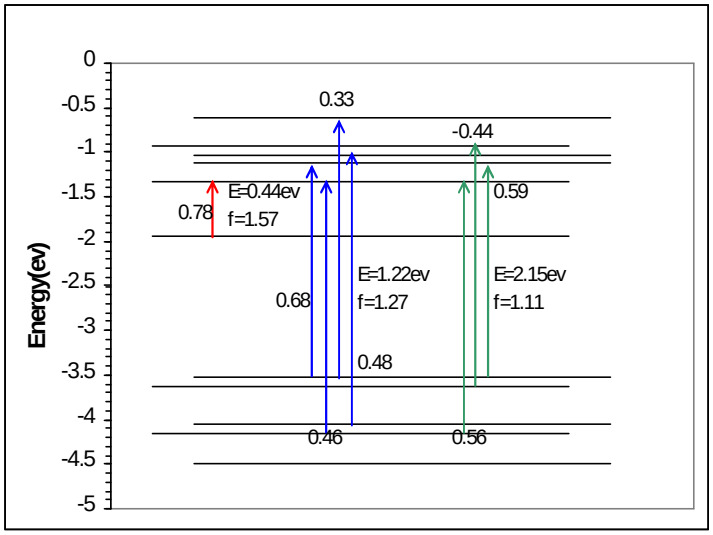

Figure 3.10: Orbital energies and excited state configurations for $12T^{-}$

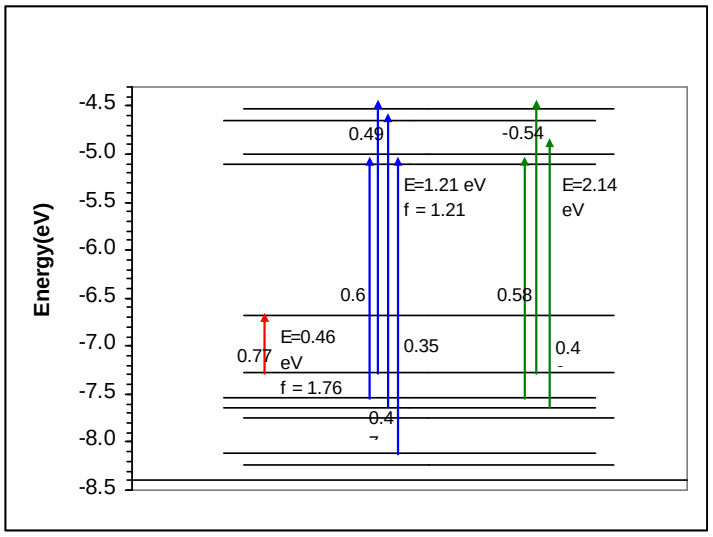

Figure 3.11: Orbital energies and excited state configurations for $12T^{+}$

3.2 UPS simulations by ΔSCF/TDDFT and DFT orbital energies (DFTϵ_n)

3.2.1 Test of methodology with different σ and π systems

Since using ΔSCF/TDDFT calculations is not a common practice in theoretical investigations of UPS experiments, ionization energies extracted from this methodology and DFTϵ_n are compared with experimental data for different σ and π systems. Model molecules chosen for this investigation are ethylene, water, ammonia and benzene which have well-resolved experimental UPS data and are good candidates for testing this new theoretical approach. Figure 3.12, 3.13 and 3.14 illustrates this comparison for ethylene, water and ammonia respectively.

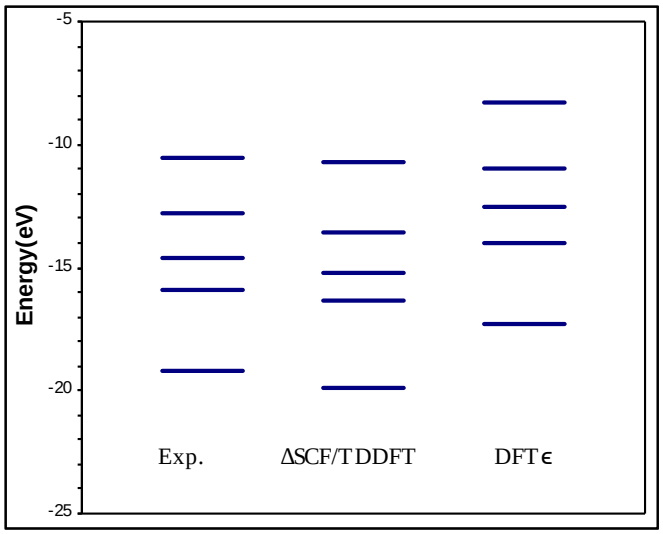

Figure 3.12: Negative IPs for ethylene obtained by ΔSCF/TDDFT and DFTϵ_n compared with experimental data.

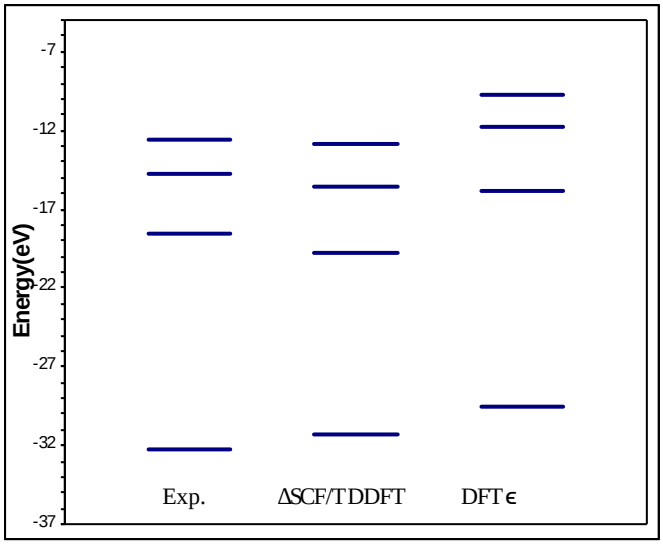

Figure 3.13: Negative IPs for water.

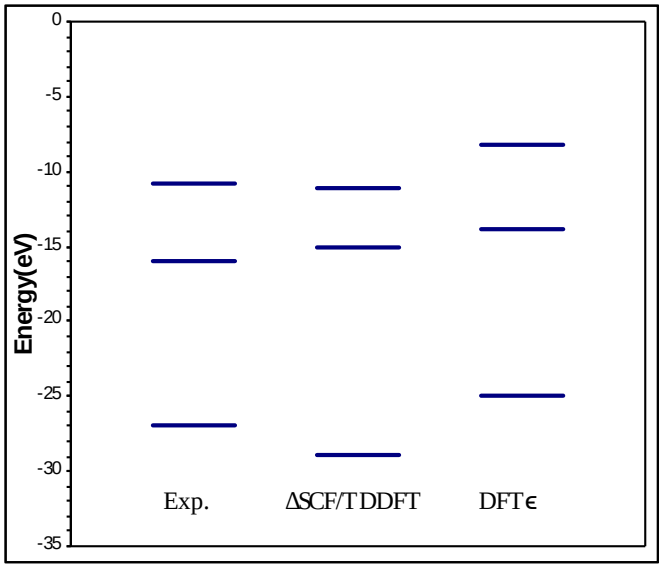

Figure 3.14: Negative IPs for ammonia.

In all three systems, ΔSCF/TDDFT is a good estimate for the first IP. In contrast, IP_2 energies predicted by ΔSCF/TDDFT are higher in water and ethylene while it is slightly lower in ammonia. The error between theoretical and experimental values gets larger for deeper-lying states. For a quantitive analysis both theoretical

and experimental values are shown in table 3.2. The errors between ΔSCF/TDDFT and experiment range in 0.2-0.3 eV for the first IP. On the other hand, negative IPs calculated by DFTϵ_n are lower than experimental data within the range 2.0-3.0 eV. This is the result of the self-interaction error present in DFT calculations. ΔSCF/TDDFT relatively corrects the results obtained by DFTϵ_n; however, the difference with experiment becomes larger for deeper-lying states, especially for water and ammonia.

	Ethylene	
DFT -ϵ	ΔSCF/TDDFT	Exp[a]
8.32(b_{3u})	10.69	10.51
10.97(b_{3g})	13.56	12.8
12.50(a_g)	15.2	14.6
13.97(b_{1u})	16.37	15.9
17.33(b_{2u})	19.93	19.2
	Water	
DFT -ϵ	ΔSCF/TDDFT	Exp[b]
9.72(b_1)	12.93	12.61
11.79($2a_1$)	15.57	14.74
15.83(b_2)	19.8	18.55
29.48($1a_1$)	31.31	32.2
	Ammonia	
DFT -ϵ	ΔSCF/TDDFT	Exp[b]
8.28($2a_1$)	11.17	10.88
13.79(e)	15.11	16
24.93($1a_1$)	28.86	27

Table 3.2: The comparison of theoretical values obtained by ΔSCF/TDDFT with orbital energies and experimental data for ethylene, water and ammonia.

a) ref. 130

b) ref. 131.

The benzene molecule is one of the most studied chemical systems in terms of UPS. Several experimental and theoretical data are present in the literature which makes this molecule a good candidate for the present investigation as well. The

comparison of DFTϵ_n and ΔSCF/TDDFT values with more recent theoretical Green function ADC(3) results and experimental UPS data using synchrotron radiation [70] is shown at Table 3.3.

DFT -ϵ.	ΔSCF/TDDFT	(ADC(3))[a]	Exp[a]
7.80($e_{1g,\pi}$)	9.53	9.16	9.45
10.53($e_{2g,\sigma}$)	12.32	12.24	11.7
10.97($a_{2u,\pi}$)	12.51	12.32	12.3
12.67($e_{1u,\sigma}$)	14.62	14.49	14.0
13.18($b_{2u,\sigma}$)	15.14	15.09	14.78
14.04($b_{1u,\sigma}$)	15.90	15.79	15.77
15.48($a_{1g,\sigma}$)	17.33	17.34	17.04

Table 3.3: Comparison of theoretical values obtained by ΔSCF/TDDFT with orbital energies, experimental data and ADC(3) Green function method for benzene.

a) ref. 70

The results clearly indicate that both ADC(3) and ΔSCF/TDDFT produce more reliable results than DFTϵ_n. ΔSCF/TDDFT gives a closer value to experiment than ADC(3) for the first IP while the difference between two theories is around 0.1 eV for deeper-lying states. The largest variations from experimental data are seen in $^2E_{2g}$ and $^2E_{1u}$ doubly degenerate cationic states for both calculations. Previous semi-empirical studies with CNDO/S3 orbital energies were also shown to be in good agreement with experiment for low-lying states [95] after applying a linear shift of 0.73 eV to all theoretical values to match the first IP with experiment. However, the accuracy of the CNDO/S3 method deteriorates for deeper-lying states above 15 eV where the relaxation effects become more essential.

3.2.2 Comparison of $\Delta SCF_{(n)}$ with ΔSCF/TDDFT in higher IPs

It is possible to calculate higher IPs with $\Delta SCF_{(n)}$ by employing symmetry constraints on the initial guess of the wave function to obtain the excited states of the ions. This method is applied to water and ethylene in order to compare the effectiveness of ΔSCF/TDDFT and $\Delta SCF_{(n)}$ for more energetic ionizations in UPS. The results are shown in Table 3.4. For ethylene, $\Delta SCF_{(n)}$ and ΔSCF/TDDFT values are almost identical. The largest difference is slightly above 0.2 eV in $^2B_{2u}$ state, where ΔSCF/TDDFT value is closer to the experiment. For the water molecule, ΔSCF/TDDFT results are 0.35 eV higher than $\Delta SCF_{(n)}$ for the cationic states $^2A_1$ and $^2B_2$. However, it is not possible to calculate the deepest-lying valence state for water since upon the interchange of orbitals $1a_1$ and b_1, (see table 3.2 for orbital symmetries) the symmetry of the wave function is $^2A_1$ as in the case of second IP. Therefore, SCF calculation falls into this state since it is lower in energy. This result illustrates the limitations of $\Delta SCF_{(n)}$ method for higher IPs, especially when the investigated system has a low symmetry.

Ethylene			**Water**		
$\Delta SCF_{(n)}$	ΔSCF/ TDDFT	Exp.	$\Delta SCF_{(n)}$	ΔSCF/ TDDFT	Exp.
10.69($^2B_{3u}$)	10.69	10.51	12.93($^2B_1$)	12.93	12.61
13.59($^2B_{3g}$)	13.56	12.80	15.12($^2A_1$)	15.57	14.74
15.03(^2A_g)	15.20	14.60	19.45($^2B_2$)	19.80	18.55
16.61($^2B_{2u}$)	16.37	15.90		31.31	32.2
20.05($^2B_{1u}$)	19.93	19.20			

Table 3.4 Comparison of $\Delta SCF_{(n)}$ and ΔSCF/TDDFT for higher IPs. Note that the first IP is calculated with ΔSCF in both methods.

3.2.3 Electronic structure calculations for monomers of heterocyclic systems: furan, pyrrole and thiophene.

The order of molecular orbitals in the heterocyclic monomers furan, pyrrole and thiophene was given in Table 1.2. In this section, a more quantitative analysis will be discussed by using the methodologies described in previous sections. Table 3.5 shows the theoretical values for valence shell ionizations in these molecules together with the experimental vertical IPs.

For all three molecules, the energies of the cationic states predicted by the negative DFTϵ_n are considerably lower than experimental values. In contrast, ΔSCF/TDDFT method constitutes a definite improvement when compared to DFTϵ_n with an increase in energy levels around 2.0 eV. However, ΔSCF/TDDFT overestimates the energies for all levels when compared to the experiment. The difference between experimental values and ΔSCF/TDDFT varies between 0.13-0.96 eV. We note that the maximum variation is for the deepest-lying valence state of thiophene.

The results of the current investigation on furan, pyrrole and thiophene are further compared with negative orbital energies at the H.F. level and the ADC(3) Green function level of theory. It can be seen that H.F. orbital energies are in good agreement with experiment for the first two IPs, however, the difference between theoretical and experimental values increases dramatically for the deep-lying states. ADC(3), on the other hand, gives more accurate results for these states when compared to H.F.

Furan

HF -ϵ.	ADC(3)[a]	DFT -ϵ.	ΔSCF/TDDFT	Exp.[b]
10.4($1a_{2,}\pi$)	8.7	7.27	9.24	9.11
10.8($2b_{1,}\pi$)	10.2	8.72	11.04	10.48
14.7($6a_1$)	13.3	11.38	13.68	13.10
15.2($5a_1$)	14.0	12.16	14.40	13.74
15.6($4b_2$)	14.3	12.42	14.67	14.46
16.5($3b_2$)	15.2	13.49	15.70	15.18
17.1($1b_{1,}\pi$)	15.5	13.63	15.80	15.44
20.0($4a_1$)	18.0	16.16	18.19	17.49

Pyrrole

HF -ϵ.	ADC(3)[a]	DFT -ϵ.	ΔSCF/TDDFT	Exp.[b]
8.1($1a_{2,}\pi$)	8.1	6.65	8.56	8.28
9.3($2b_{1,}\pi$)	8.8	7.58	9.78	9.26
14.2($6a_1$)	13.0	11.23	13.40	12.74
15.0($4b_2$)	13.6	11.68	13.86	12.94
15.4($1b_{1,}\pi$)	13.0	12.17	13.57	13.48
15.8($3b_2$)	14.5	12.70	14.85	14.29
16.2($5a_1$)	14.8	12.85	15.03	14.76
20.1($4a_1$)	17.9	16.09	17.81	17.44

Thiophene

HF -ϵ.	ADC(3)[a]	DFT -ϵ.	ΔSCF/TDDFT	Exp.[b]
8.8($1a_{2,}\pi$)	8.7	7.48	9.29	8.96
9.4($2b_{1,}\pi$)	9.0	7.91	10.09	9.58
12.9($6a_1$)	11.9	10.57	12.72	12.04
14.2($1b_{1,}\pi$)	12.4	11.47	13.05	12.49
14.4($4b_2$)	13.3	11.79	13.89	13.15
15.0($5a_1$)	13.6	11.90	13.95	13.71
15.6($3b_2$)	14.2	12.51	14.56	14.26
	17.0	15.34	17.48	16.52

Table 3.5: Tabulated vertical IPs for furan, pyrrole and thiophene calculated by HF, ADC(3) green function, DFTϵ_n and ΔSCF/TDDFT along with experimental values.

a) ref. 103
b) ref. 33

The difference between ADC(3) Green function and ΔSCF/TDDFT results are usually within the range of 0.5 eV. In all three molecules, experimental values for the first two cationic states lie between these two methods as ΔSCF/TDDFT slightly

overestimates vertical IPs whereas ADC(3) underestimates them. For the deeper-lying states, ADC(3) tends to be in better agreement with experiment except for $5a_1$ level in pyrrole. The mean error of ΔSCF/TDDFT and ADC(3) for the tabulated values are 0.5 eV and 0.2 eV respectively. The comparison of these two methods along with DFTϵ_n is illustrated for furan, pyrrole and thiophene in Figures 3.15, 3.16 and 3.17 respectively. The results show that although DFTϵ_n are remarkably low, the spacing of energy levels is very similar with both ADC(3) and ΔSCF/TDDFT methods as well as with experimental data except for the $1b_1(\pi)$ level for pyrrole. It should be noted that the order of this level in the electronic structure is predicted differently when we move from DFTϵ_n to ΔSCF/TDDFT.

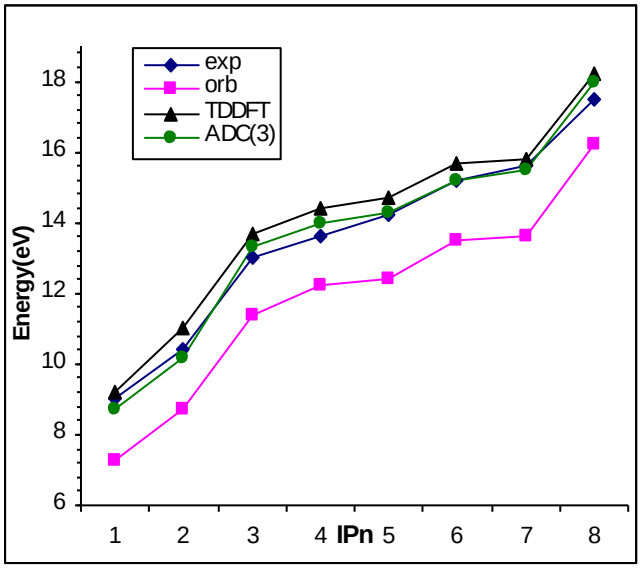

Figure 3.15: Comparison of ΔSCF/TDDFT vertical excitations, DFT orbital eigenvalues and ADC(3) energy levels with experimental vertical IPs for furan.

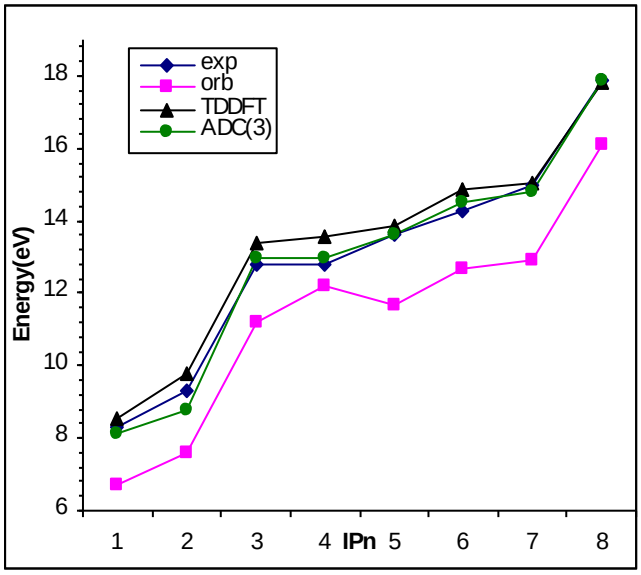

Figure 3.16: Comparison of ΔSCF/TDDFT vertical excitations, DFT orbital eigenvalues and ADC(3) energy levels with experimental vertical IPs for pyrrole.

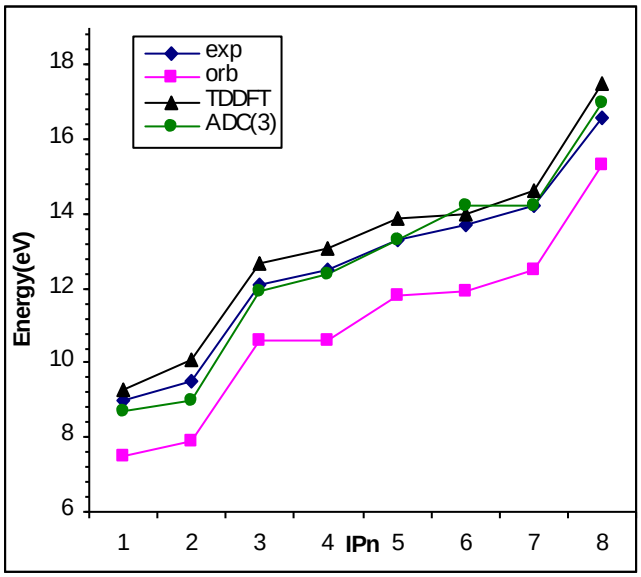

Figure 3.17: Comparison of ΔSCF/TDDFT vertical excitations, DFT orbital eigenvalues and ADC(3) energy levels with experimental vertical IPs for thiophene.

3.2.4 Oligomers of furan and thiophene.

a) Oligothiophenes (2-5)

The theoretical (Δ SCF/TDDFT) and experimental spectra for oligomers of thiophene are shown in figure 3.18a and 3.18b respectively.

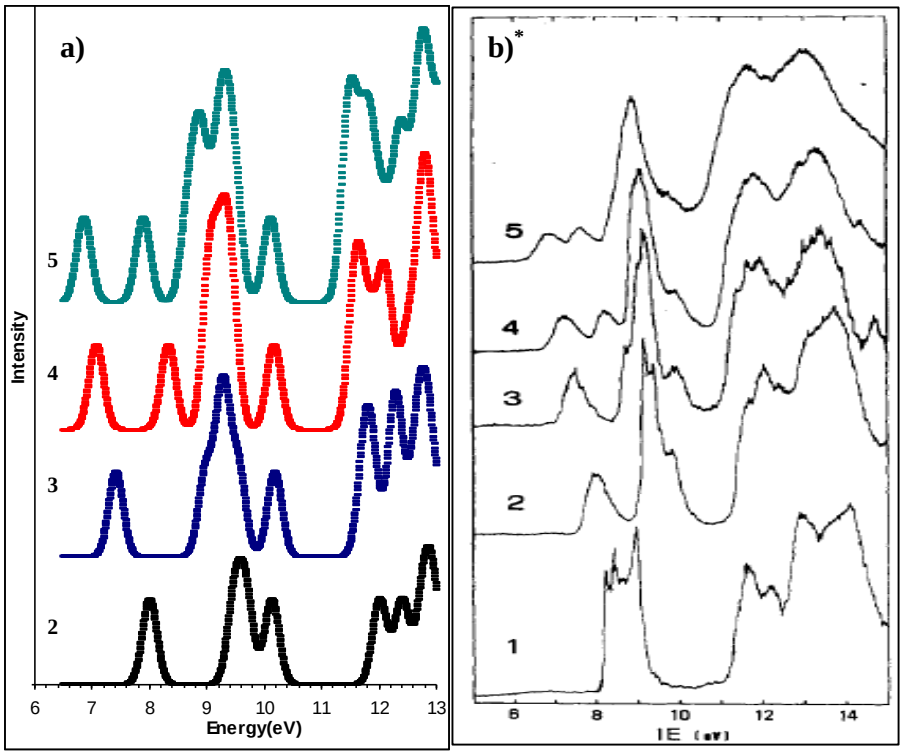

Figure 3.18: a) Theoretical and b) experimental UPS of oligothiophenes

* Reprinted figure with permission from ref. 67. Copyright (1990) by the American Chemical Society.

In the experimental spectra, the first peak associated with IP_1 shifts to lower energy as the chain length increase. The same trend is predicted from theory. Additionally, the new feature which arises after first peak in 4T and 5T is more intense in theoretical spectra. In 2T, the first peak around 8eV is followed by a more intense band with a shoulder at the end at 9-10 eV and the position of the band

changes very slightly as the chain length increases. These features are also shown in theoretical spectra except for 2T where this band is predicted to be at higher energies. Above 10 eV, comparison of theory with experiment becomes problematic since a broad feature arises in all chain lengths. However, the position and width of this feature predicted by theory is generally in good agreement with experiment.

b) Oligofurans (2-4)

Theoretical and experimental spectra of oligofurans with unit numbers 2-4 are shown in Figure 3.19a and 3.19b.

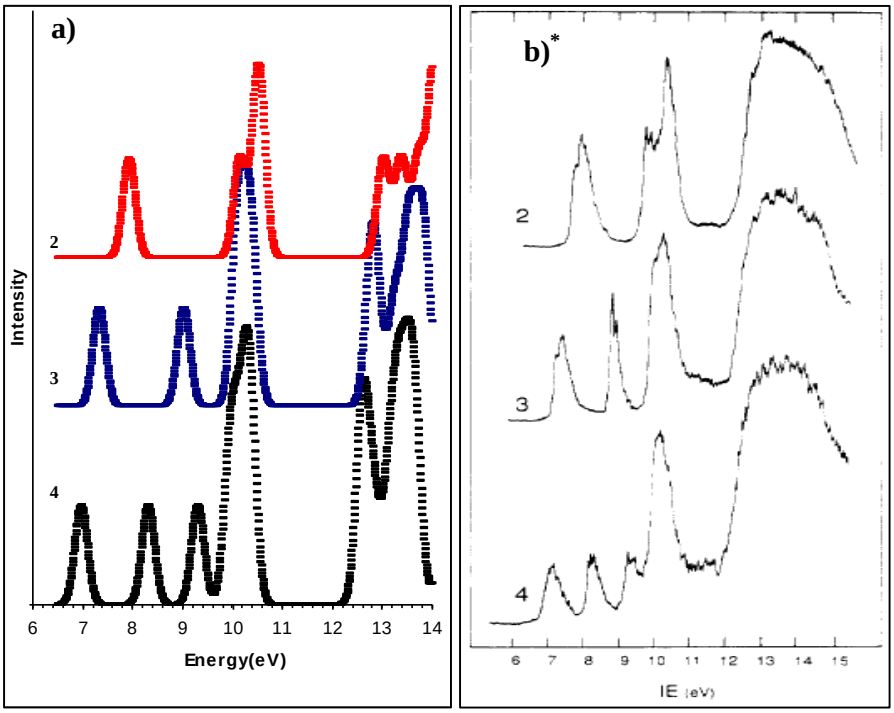

Figure 3.19: a) Theoretical and b) experimental UPS of oligofurans (2-4)

* Reprinted figure with permission from ref. 68. Copyright (1991) by the American Chemical Society.

The experimental spectrum of 2F is similar to that of 2T with a peak at 8 eV, followed by a more intense and a broad band. The first peak associated with the first IP shifts to lower energies with increasing chain length as in the case of oligothiophenes. These features are clearly reproduced in theoretical spectra as well. Additionally, the new bands and their energies in 3F and 4F are in very good agreement with experiment. The comparison of theoretical and experimental spectra becomes difficult once again as a very broad feature arise around 12 eV for all oligomers.

In order to make a more quantitive analysis on the performance of ΔSCF/TDDFT, theoretical IP values are compared with experimental data which could be extracted from UPS. Tabulated values are shown for oligothiophenes and oligofurans in Tables 3.6 and 3.7 respectively. It can be seen that the agreement between ΔSCF/TDDFT and experiment is quite good and within the range of 0.2 eV for most cases. The largest variation is 0.35 eV for IP_4 in 2T. It should also be stated that the agreement with experiment and theory for oligomers is better when compared to the monomers (Table 3.5) and ΔSCF/TDDFT method actually seems to work better on larger systems.

2T			**3T**		
DFT -ϵ.	ΔSCF/TDDFT	Exp.[a]	DFT -ϵ.	ΔSCF/TDDFT	Exp.
6.59	8.00	7.95	6.23	7.38	7.43
7.94	9.48	9.16	7.69	8.94	8.77
8.14	9.68	9.35	7.98	9.22	9.05
8.65	10.13	9.78	8.09	9.26	9.23
10.42	12.01	11.5-…*	8.27	9.51	-
10.82	12.40		9.14	10.14	9.88
11.26	12.78		10.42	11.70	11.2-…
11.41	12.94		10.59	11.82	
11.96	13.41		10.95	12.21	
12.14	13.44		11.18	12.28	
12.19	13.66		11.44	12.60	
			11.67	12.72	
			11.88	12.85	
			12.02	13.19	
4T			**5T**		
6.04	7.07	7.28	5.93	6.85	7.11
7.13	8.32	8.25	6.77	7.88	7.85
8.00	9.04	9.1	7.76	8.66	8.7
8.07	9.06	-	8.01	8.84	-
8.21	9.27	9.20	8.06	8.92	-
8.29	9.32	9.3	8.16	9.17	9.18
8.38	9.44	-	8.28	9.27	-
9.40	10.17	9.92	8.37	9.37	-
10.43	11.57	11.0-…	8.73	9.49	-
10.53	11.63		9.56	10.11	9.97
10.72	11.83		10.44	11.45	10.9-…
11.03	12.05		10.50	11.47	
11.13	12.15		10.62	11.62	
11.41	12.47		10.81	11.79	
11.68	12.71		11.09	11.85	
11.73	12.79		11.11	12.08	
11.75	12.81		11.39	12.33	
12.12	12.96		11.55	12.40	
12.20	13.17		11.71	12.63	
			11.79	12.73	
			11.82	12.79	
			12.01	13.07	
			12.17	13.11	

Table 3.6: Tabulated vertical IP for oligothiophenes (2-5) calculated with negative DFT orbital energies and ΔSCF/TDDFT along with experimental values.

a) ref. 67

*) a broad band develops at this point of the spectra.

2F			**3F**		
DFT -ϵ.	ΔSCF/TDDFT	Exp.[a]	DFT -ϵ.	ΔSCF/TDDFT	Exp.
6.41	7.92	7.87	6.05	7.33	7.33
8.44	10.14	9.73	7.56	9.02	8.75
8.88	10.49	10.27	8.77	10.07	10.0
8.95	10.55	-	8.90	10.15	-
11.35	13.02	12.4-…	9.03	10.30	10.20
11.70	13.38		9.23	10.40	-
12.08	13.73		11.40	12.77	12.3-…
12.41	14.03		11.52	12.86	
12.42	14.05		11.86	13.23	
			12.10	13.47	
			12.27	13.59	
			12.43	13.76	
			12.52	13.87	
			13.11	14.46	

4F		
5.86	6.98	7.08
7.00	8.32	8.22
8.20	9.32	9.30
8.87	9.94	-
8.95	10.05	10.10
9.02	10.22	-
9.13	10.33	10.35
9.43	10.38	-
11.44	12.61	12.0-…
11.48	12.62	
11.66	12.83	
11.96	13.14	
12.11	13.29	
12.24	13.37	
12.35	13.52	
12.48	13.60	
12.55	13.71	
13.14	14.28	

Table 3.7: Tabulated vertical IP for oligofurans (2-4) calculated with negative DFT orbital energies and ΔSCF/TDDFT along with experimental values.

a) ref. 68

One problem with the ΔSCF/TDDFT values in Tables 3.5 and 3.6 is that they decrease too fast with increasing chain length when compared to experiment. In order to see if there is a convergence in longer chains, ΔSCF/TDDFT values are obtained for oligothiophenes up to 12 units. As shown in Figure 3.20, the values are convergent in longer chain limit. The difference between 12T and 11T is 0.04 eV. In contrast, the decrease in experimental IP_1 with chain length is slower. This can be explained by the presence of rotamers which have been reported to alter the IPs slightly in longer chains. [67]

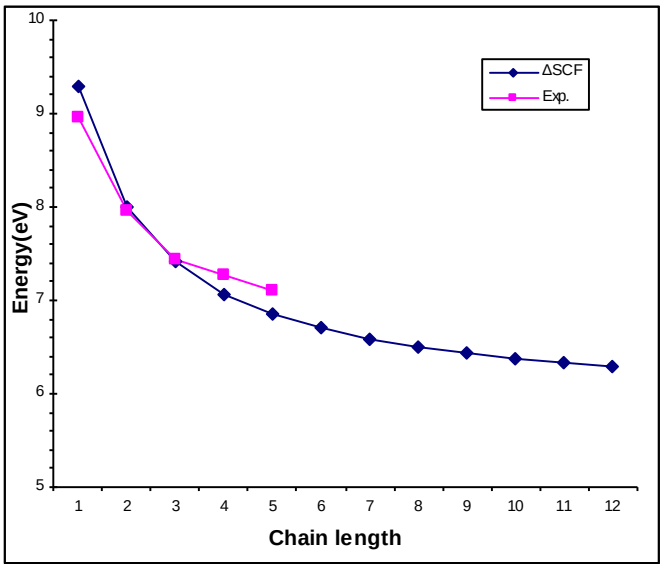

Figure 3.20: ΔSCF values and experimental first IPs for oligothiophenes (1-12)

The theoretical prediction of UPS in conjugated oligomers has been studied previously with VEH theory. [65, 77] The results of theoretical calculations are usually shown to be in good agreement with experiment; however, energy levels were shifted by 3.3 eV [77] to account for polarization effects in solid state which is in fact in the range of 0.8-1.2eV for thiophene oligomers. [66, 67] In contrast,

ΔSCF/TDDFT data which compared with gas phase spectra seems to be a good fit to the experimental data without any shifts or contractions.

3.1.5 DFTϵ_n for longer systems

The previous investigations in this study have indicated that although IPs predicted by DFTϵ_n are too low, the spacing between energy levels are generally in good agreement with the experiment. In this aspect, we present the simulated UPS of thiophene and furan oligomers in Figures 3.21 and 3.22 respectively.

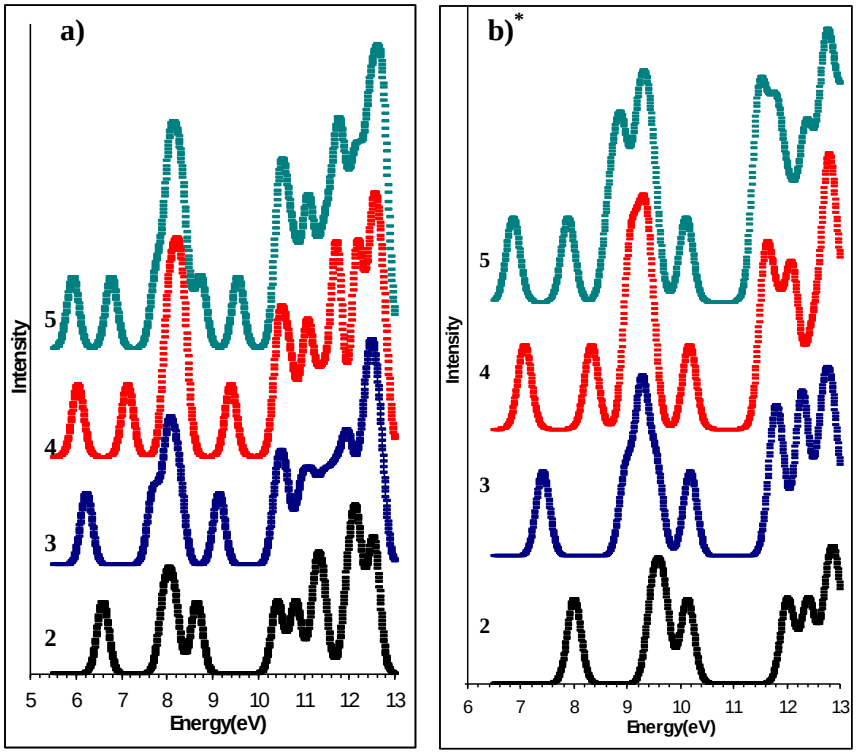

Figure 3.21: Theoretical UPS of thiophene (2-5) obtained by a) DFTϵ_n and b) ΔSCF/TDDFT.

* ΔSCF/TDDFT spectra are again shown in this page to ease the comparison

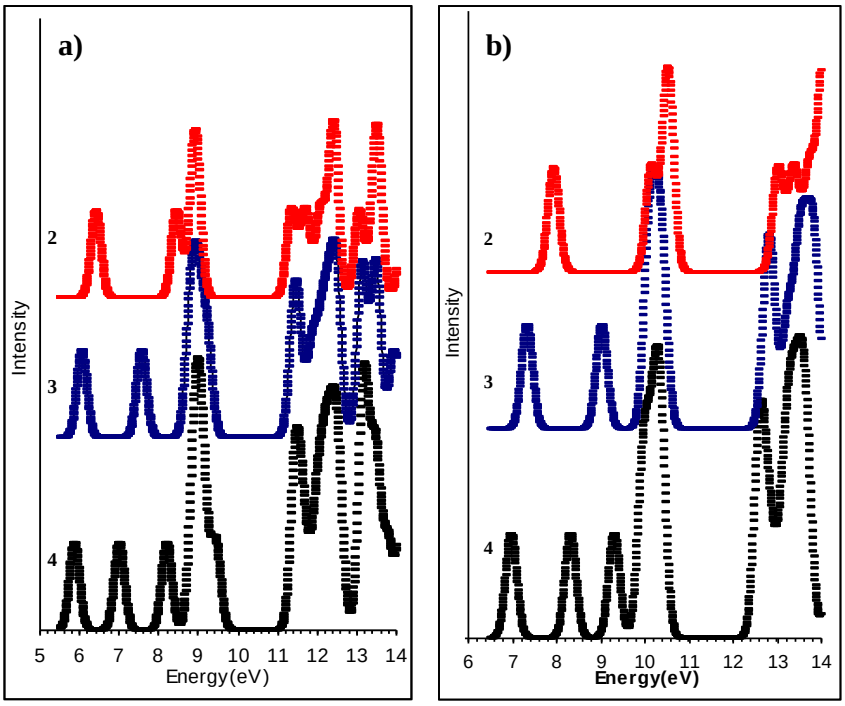

Figure 3.22: Theoretical UPS of furan (2-4) obtained obtained by a) DFTϵ_n and b) ΔSCF/TDDFT.

When we compare the spectra obtained from DFTϵ_n with experiment and ΔSCF/TDDFT (Figures 3.18 and 3.19), we see that the order of peak positions and intensities are generally in good agreement between two methods. On the other hand, energies of the peaks are lower than both experiment and ΔSCF/TDDFT as in the case of monomers.

Table 3.5 and 3.6 show that the energy difference between DFTϵ_n and ΔSCF/TDDFT is very similar for all energy levels in the same system. This relation is illustrated in Figure 3.23 by displaying discrete energy levels obtained from ΔSCF/TDDFT and DFTϵ_n for 5T. In order make a better comparison; all the energy levels obtained from DFTϵ_n are shifted to higher energies by 0.92 eV (The energy difference in two methods for the first IP). As we can see, after the shifting of the

DFTϵ_n values, there is a good agreement between these two methods except for the energy levels lying in the interval 9.5-10.5 eV.

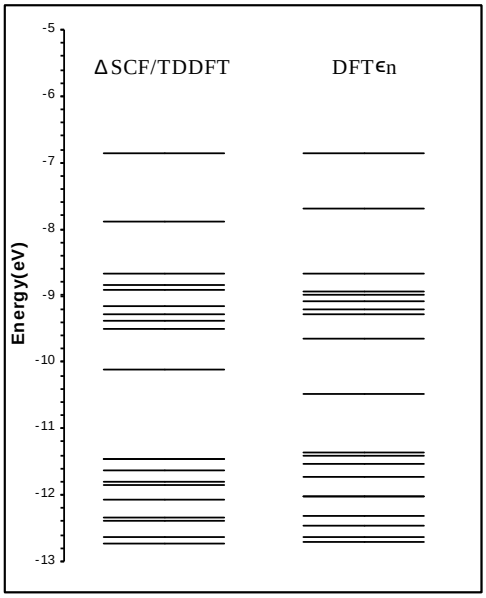

Figure 3.23: Comparison of energy levels in 5T obtained by ΔSCF/TDDFT and DFTϵ_n

From the values in Tables 3.5 and 3.6, we see that the energy difference between ΔSCF/TDDFT and DFTϵ_n gets smaller as the chain length increases. In this aspect, we compare the first IPs obtained from these two methods for the longer oligomers of thiophene in order to account the effects of system size. The results are shown in Figure 3.24. It can be seen that as we move to longer chains, the difference between ΔSCF and HOMO energies get smaller in a convergent way. We note that the differences vary in the range 1.81eV-0.58 eV. We further calculate the difference in long chain limit by extrapolating the IP energies using a second order polynomial fit. It is seen that the difference converges to 0.38 eV. The fact that ΔSCF/TDDFT

and DFTϵ_n values gets closer in longer chains could be rationalized by the decrease in self-interaction error in DFTϵ_n with increasing system size.

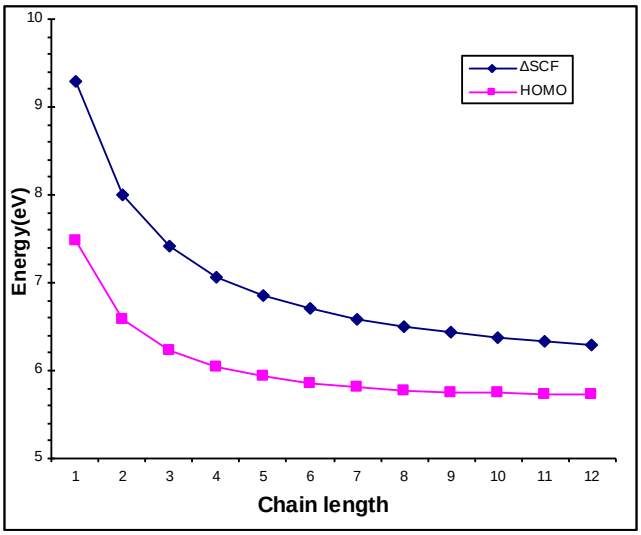

Figure 3.24: Δ SCF (IP1) values and negative Homo energies for oligomers of thiophene (1-12)

3.2.6 Secondary excitations (shake-up satellites) in ΔSCF/TDDFT.

In the methods section we describe which excited states of cations corresponds to cationic states observed during UPS experiment. These states are dominated by nβ→(LUMO)β configuration. However, there are additional multi-configurational excited states of cations predicted at the TDDFT level of theory which include different configurations along with nβ→(HOMO)β configuration with a comparable CI expansion coefficient. These states could be interpreted as satellite states in UPS. Such a state where ionization mix with HOMO→LUMO excitation in TDDFT picture is illustrated in Figure 3.25.

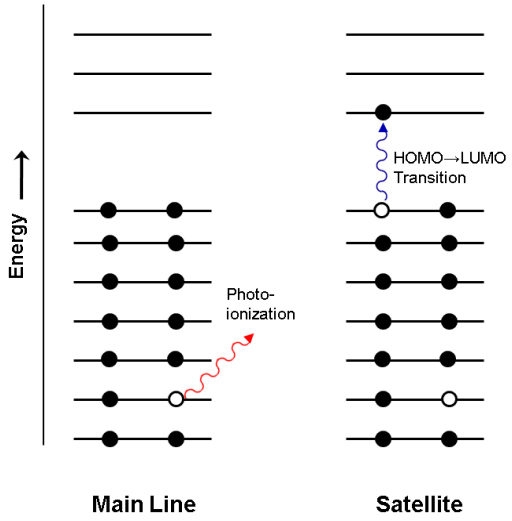

Figure 3.25: Illustration of the main line and a secondary excitation associated with HOMO→LUMO excitation

The satellite peaks in monomers thiophene, pyrrole and furan have been studied previously by ADC(3) [33, 103] and SAC-CI [102] methods. In table 3.6, we present the energies and relative intensities of main line and satellite lines for $1b_1^{-1}(\pi)$ level in these monomers obtained by TDDFT along with these methods. The intensities of lines are obtained using simple overlap approximation ($I = \left\langle \Psi^0 \middle| \Psi^+ \right\rangle$) [132, 133] which relates the CI coefficients with satellite intensities. For thiophene, TDDFT predicts mainly a one electron transition with two weak satellites at 14.53 eV and 15.79 eV for $1b_1^{-1}(\pi)$ level. SAC-CI and ADC(3) predicts similar characteristics for this state. However, the main line intensity is lower than with TDDFT. The splitting of the $1b_1^{-1}(\pi)$ level of pyrrole is more severe in TDDFT as two satellite lines are predicted at 14.35 eV and 15.75 eV with significant intensities. The theoretical values lie close for the second satellite line, however, TDDFT predicts a lower value for the third line than ADC(3) and SAC-CI. For pyrrole, there is also experimental value for the $1b_1^{-1}(\pi)$ satellite at 16.62 eV.

	Thiophene		
Configuration	TDDFT*	SAC-CI[a]	ADC(3)[b]
$1b_1^{-1}(\pi)$	13.05 (0.90)	12.56 (0.61)	12.52 (0.57)
	14.53 (0.05)	14.78 (0.08)	13.83 (0.15)
	15.79 (0.08)	16.19 (0.11)	15.46 (0.12)
	Pyrrole		
$1b_1^{-1}(\pi)$	13.57 (0.65)	12.77 (0.49)	12.73 (0.30)
	14.35 (0.10)	14.70 (0.19)	14.26 (0.42)
	15.75 (0.25)	17.01 (0.07)	16.50 (0.09)
	Furan		
$1b_1^{-1}(\pi)$	14.39 (0.24)	14.03 (0.26)	13.23 (0.09)
	15.70 (0.44)	15.84 (0.45)	15.64 (0.69)
	16.81 (0.33)	17.97 (0.10)	17.37 (0.06)

Table 3.6: Comparison of the satellite structure of $1b_1$ peak predicted by TDDFT, SAC-CI and ADC(3) level of theories. Intensities are shown in paranthesis.

a) ref. 102

b) ref. 33

*) intensities are obtained by taking the square of CI coefficients of $n\beta \rightarrow (HOMO)\beta$ transition

For furan, TDDFT and SAC-CI predicts a multi-electron transition $1b_1^{-1}(\pi)$ level whereas ADC(3) predicts mainly a one electron picture with weak features. However, the theoretical results of TDDFT and SAC-CI are also confirmed by EMS experiment as it shows two peaks at energies 13.6eV and 15.6eV with equal intensities for this level. [82]

Chapter 4: Analysis and conclusion

In this study, we present the theoretical simulation of UV-vis and UPS for conjugated systems by employing DFT. In the first part, we have investigated the geometries and excited states of oligothiophenes. In the absence of counter-ions, anionic defects in oligothiophenes were found to be delocalized while they were more localized when counter-ions are introduced to the system. However, the sub-band transitions with delocalized geometry agree with experiment, therefore, we conclude that the nature of transitions is not linked with defect localization.

For the short oligomers, there are two sub-band transitions were found while an additional transition appeared in the longer systems. The energies and intensities of these excitations change considerably with the system size. Therefore, we conclude that spectral changes should occur in long chain lengths.

We found that the first excited state mainly arises from a one electron transition. On the other hand, the second and third excited states have notable multi-configurational character. These findings contradict with polaron picture where all three sub-band transitions were shown to be a one electron process.

When the excitation energies of anions and cations are compared, we have found almost identical UV spectra for these systems. Therefore, perfect electron-hole symmetry is confirmed for oligothiophenes in DFT level. However, investigation of energy levels and electronic transitions indicate that the origin of electron-hole symmetry in DFT level is very different than the predictions of polaron-bipolaron model.

For the second part, we have introduced a new methodology, ΔSCF/TDDFT, in order to calculate the cationic states of conjugated systems observed in the UPS experiment. For the heterocyclic monomers, we found that the agreement between energy levels and experimental data is around 0.5 eV while the method seems to work better in longer chain lengths. The agreement with experimental data is within the range of 0.2 eV for most of the valence states in the oligomers of furan and thiophene.

The problem with previous semi-empirical and VEH studies is that the energy levels are exposed to several eV shifts and contractions in order to match the theory and experiment. On the other hand, the comparison of simulated theoretical spectra with experimental gas phase data indicates that ΔSCF/TDDFT can successfully describe the valence region of UPS in furan and thiophene oligomers without any shifts or contractions.

One main issue with ΔSCF/TDDFT results is the relatively fast decrease of the first IP when compared to the experiment. This could be the result of an experimental disorder.

We extend our discussion of theoretical UPS simulations by using DFTϵ_n. It is found that IP energies predicted in DFT level suffer from self-interaction error considerably in small systems while the error between DFTϵ_n and experiment becomes smaller with increasing the system size. However, for all of the investigated systems, spacing of DFT orbital energies is in good agreement with both ΔSCF/TDDFT and experiment. Therefore, we conclude that DFTϵ_n could be safely used in simulation of UPS of conjugated systems with a systematic shift which depends on the system size.

We also show that the descriptions of shake-up (satellite) excitations are dealt properly in ΔSCF/TDDFT methodology. The energies and intensities of the satellite lines in ΔSCF/TDDFT level were compared with the results of SAC-CI and ADC(3) investigations for $1b_1(\pi)$ level in heterocyclic monomers. We found that for furan and pyrrole, severe shake-up contamination is predicted using all three methods. However, the energies and the intensities of the satellite lines show a considerable variation within theoretical predictions.

Chapter 5: References

1. H. Shirakawa, E. J. Louis, A. G. MacDiarmid, C. K. Chiang, A. J. Heeger, J. Chem. Soc., Chem. Comm., 16, (1977) 578.
2. C.T. Chen, Chem. Mater., 16, (2004) 4389.
3. A. P. Kulkarni, C. J. Tonzola, A. Babel, and S. A. Jenekhe, Chem. Mater., 16, (2004) 4556.
4. M. L. Chabinyc, A. Salleo, Chem. Mater., 16, (2004) 4509.
5. A. A. Argun, P.H. Aubert, B. C. Thompson, I. Schwendeman, C. L. Gaupp, J. Hwang, N. J. Pinto, D. B. Tanner, A. G. MacDiarmid, J. R. Reynolds, Chem. Mater., 16, (2004) 4401.
6. M. Ozaki, D. L. Peebles, B. R. Weinberger, C. K. Chiang, S. C. Gau, A. J. Heeger, A. G. MacDiarmid, Appl. Phys. Lett., 35, (1979) 83.
7. S. Güneş, H. Neugebauer, N. S. Sariçiftci, Chem. Rev., 107, (2007) 1324.
8. K. M. Coakley, M. D. McGehee, Chem. Mater., 16, (2004) 4533.
9. R. H. Friend, G. J. Denton, J. J. M. Halls, N. T. Harrison, A. B. Holmes, A. Kökhler, A. Lux, S. C. Moratti, K. Pichler, N. Tessler, K. Towns, Synt. Met., 84, (1997) 463.
10. J. L. Brédas, C. Adant, P. Tackx, A. Persoons, Chem. Rev., 94, (1994) 243.
11. T. A. Skotheim, R. L. Elsenbaumer, J. R Reynolds, Handbook of Conducting Polymers; 2nd ed. Eds. Marcel Dekker, Inc.: New York, 1997, 1097.
12. H. Naarmann, N. Theophilou, Synth. Met., 22, (1987) 1.
13. H. Naarmann, Synth. Met., 17, (1987) 2233.
14. A. O. Patil, A. J. Heeger, F. Wudl, Chem. Rev., 88, (1988) 183.

15. M. J. Bielefeld, D. D. Fitts, J. Am. Chem. Soc., 88, (1966) 4804.
16. K. K. Kanazawa, A. F. Diaz, R. H. Geiss, W. D. Gill, J. F. Kwak, J. A, Loean, J. F. Rabolt, G. B. Street, J. Chem. Soc., Chem. Commun., (1979) 854.
17. M. R. Bryce, A. Chissel, P. Kathirgamanathanan, D. Parker, N. R. M. Smith, J. Chem. Soc., Chem. Commun., (1987) 466.
18. T.-C. Chung, J. H. Kaufman, A. J. Heeger, F. Wudl, Phys. Rev. B., 30, (1984) 702.
19. M. J. Gonzalez-Tejera, E. Sanchez de la Blanca, I. Carrillo, Synthetic Metals, 158, (2008) 165.
20. G. Tourillon, F. Garnier, J. Electroanal. Chem., 135, (1982) 173.
21. S. Pons, A. S, Hinman, Electrochem. Acta, 29, (1984) 1251.
22. K. Müllen, G. Egner, Electronic Materials: The Oligomer Approach, Eds.; Wiley-VCH: Weinheim, 1998.
23. J. M. Tour, Chem. Rev., 96, (1996) 537.
24. R. E. Martin, T. Mäder, F. Diederich, Angew. Chem. Int. Ed., 38, (1999) 817.
25. J. L. Brédas, R. Silbey, D. S. Boudreaux, R. R. Chance, J. Am. Chem. Soc., 105, (1983) 6555.
26. J. Guay, P. Kasai, A. Diaz, R. Wu, J. M. Tour, L. H. Dao, Chem. Mater., 4, (1992) 1097.
27. W. R. Salaneck, R. H. Friend, J. L. Bredas, Physics Reports, 319, (1999) 231
28. P. J. Derrick, L. Asbrink, O. Edqvist, B.-O. Jonsson, and E. Lindholm, Int. J. Mass Spectrom. Ion Phys., 6, (1971) 161.
29. E. E. Rennie, C. A. F. Johnson, J. E. Parker, D. M. P. Holland, D. A. Shaw, M. A. MacDonald, M. A. Hayes, L. G. Shpinkova, Chem. Phys., 236, (1998) 365.
30. M. H. Palmer, I. C. Walker, M. F. Guest, Chem. Phys., 238, (1998) 179.

31. M. H. Palmer, I. C. Walker, C. C. Ballard, M. F. Guest, Chem. Phys., 192, (1995) 111.

32. M. H. Palmer, I. C. Walker, M. F. Guest, Chem. Phys., 241, (1999) 275.

33. D. M.P. Holland, L. Karlsson, W. Von Niessen, Journal of Electron Spectroscopy and Related Phenomena, 113, (2001) 221.

34. W. P. Su, J. R. Schrie!er, A. J. Heeger, Phys. Rev. Lett., 42, (1979) 1698.

35. A. J. Heeger, S. Kivelson, J. R. Schrie!er, W. P. Su, Rev. Mod. Phys., 60, (1988) 781.

36. N. Suzuki, M. Ozaki, S. Etemad, A. J. Heeger, A. G. MacDiarmid, Phys. Rev. Lett., 45, (1980) 1483.

37. J. H. Kaufman, T. C. Chung, A. J. Heeger, J. Electrochem. Soc., 131, (1984) 2092.

38. K. Yakushi, L. J. Lauchlan, T. C. Clarke, G. B. Street, J. Chem. Phys., 79, (1983) 4774.

39. J. Fink, B. Scheerer, W. Wernet, M. Monkenbusch, G. Wegner, H. J. Freund, H. Gonska, Phys. Rev. B, 34, (1986) 1101.

40. P. Pfluger, M. Krounbi, G. B. Street, G. Weiser, J. Chem. Phys., 78, (1983) 3212.

41. W. P. Su, J. R. Schrieffer, A. Heeger, Phys. Rev. B, 22, (1980) 2099

42. J. L. Bredas, G. B. Street, Acc. Chem. Res. 18, (1985) 319.

43. J. L. Bredas, R. R. Chance, R. Silbey, Phys. Rev. B, 26, (1982) 5843.

44. J. L. Bredas, R. R. Chance, R. Silbey, G. Nicolas, P. Durand, J. Chem. Phys., 75, (1981) 255.

45. M. J. Rice, Phys. Lett. A, 71, (1979) 152.

46. S. A. Brazovskii, N. Kirova, JEPT Lett., 33, (1981) 1.

47. S. Stafstrom, J. L. Bredas, Phys. Rev. B., 38, (1988) 4180.

48. J. L. Bredas, F. Wudl, A. J. Heeger, Solid State Commun., 63, (1987) 577.

49. J. L. Bredas, J. C. Scott, K. Yakushi, G. B. Street, Phys. Rev. B, 30, (1984) 1023.

50. D. S. Boudreaux, R. R. Chance, J. L. Bredas, R. Silbey, Phys.Rev. B, 28, (1983) 6927.

51. C. Ehrendorfer, A. Karpfen, J. Chem. Phys., 99, (1995) 10196.

52. D. Bertho, C. Jouanin, Phys. Rev. B, 35, (1987) 626.

53. P. Bauerle, U. Segelbacher, K.-U. Gaudl, D. Huttenlocher, M. Mehring, Angew. Chem., Int. Ed. Engl., 32, (1993) 76.

54. D. Fichou, G. Horowitz, B. Xu, F. Garnier, Synth. Met., 39, (1990) 243.

55. M. G. Hill, K. R. Mann, L. L. Miller, J.-F. Penneau, J.Am. Chem. Soc., 114, (1992) 2728.

56. P. Bauerle, U. Segelbacher, A. Maier, M. Mehring, J. Am.Chem. Soc., 115, (1993) 10217.

57. T. Keszthelyi, M. M.-L. Grage, J. F. Offersgard, R. Wilbrandt, C. Svendsen, O. S. Mortensen, J. K. Pedersen, H. J. A. Jensen, J. Phys. Chem. A, 104, (2004) 2808.

58. M. Rubio, E. Orti, R. Pou-Amerigo, M. Merchan, J. Phys.Chem. A, 105, (2001) 9788.

59. U. Salzner, J. Chem. Theory Comput., 3, (2007) 1143.

60. S. Okur, U, Salzner, J. Phys. Chem. A, 46 (2008) 112.

61. G. Iucci, K. Xing, M. Loegdlund, M. Fahlman, W. R. Salaneck, Chem. Phys. Lett., 244, (1995) 139.

62. W. R. Salaneck, H. R. Thomas, R. W. Bigelow, C. B. Duke, E. W. Plummer, A. J. Heeger, and A. G. MacDiarmid, J. Chem. Phys., 72, (1980) 3674.

63. W. R. Salaneck, H. R. Thomas, C. B. Duke, E. W. Plummer, A. J. Heeger and A. G. MacDiarmid, Synthetic Metals, 1(1980), 133.

64. P. Dannetun, M. Loegdlund, C. W. Spangler, J. L. Bredas, and W. R. Salaneck, J. Phys. Chem., 98 (1994) 2853.

65. M. Loegdlund, P. Dannetum, C. Fredriksson, W. R. Salaneck, J. L. Bredas, Phys. Rev. B, 53 (1996), 16327.

66. A. Chandekar, J. E. Whitten, Synthetic Metals, 150 (2005), 259

67. D. Jones, M. Guerra, L. Favaretto, A. Modelli, M. Fabrizio, and G. Distefano, J. Phys. Chem., 94, (1990) 5761.

68. G. Distefano, D. Jones, M. Guerra, L. Favaretto, A. Modelli and M. Guerra, J. Phys. Chem., 95, (1991) 9746.

69. I. Powis, I. L. Zaytseva, A. B. Trofimov, J. Schirmer, D. M. P. Holland, A. W. Potts, and L. Karlsson, J. Phys. B: At. Mol. Opt. Phys., 40, (2007) 2019.

70. A. B. Trofimov, J. Schirmer, D. M. P. Holland, L. Karlsson, R. Maripuu, K. Siegbahn, and A. W. Potts, Chem. Phys., 263, (2001) 167.

71. A. W. Potts, A. B. Trofimov, J. Schirmer, D. M. P. Holland, and L. Karlsson, Chem. Phys., 271, (2001) 337.

72. T. Koopmans, "Ordering of Wave Functions and Eigenvalues to the Individual Electrons of an Atom.", Physica, 1, (1933) 104.

73. W. R. Salaneck, In Handbook of Conducting Polymers; T. A. Skotheim, Ed.; Dekker: New York, 1986; Vol. 2, p 1337.

74. Y. Harada, S. Masuda, and H. Ozaki, Chem. Rev., 97, (1997) 1897.

75. N. Sato, K. Seki, and H. Inokuchi, J. Chem. Soc. Faraday Trans.2, 77 (1981), 1621.

76. M. Fahlman, M. Loegdlund, S. Stafstroem, W. R. Salaneck, R. H. Friend, P. L. Burn, A. B. Holmes, K. Kaeriyama, Y. Sonoda, F. Meyers, and J. L. Bredas, Macromolecules, 28, (1995) 1959.
77. J. Cornil, S. Vanderdonckt, R. Lazzaroni, D. A. dos Santos, G. Thys, H. J. Geise, L.-M. Yu, M. Szablewski, D. Bloor, M. Lögdlund, W. R. Salaneck, N. E. Gruhn, D. L. Lichtenberger, P. A. Lee, N. R. Armstrong, and J. L. Brédas, Chem. Mater., 11, (1999) 2439.
78. P. Keane, A. N. de Brito, N. Correia, S. Svensson, L. Karlsson, B. Wannberg, U. Gelius, S. Lunell, W. R. Salaneck, M. Lögdlund, D. B. Swanson, A. G. MacDiarmid, Phys. Rev. B, 45, (1992) 6390.
79. B. Sjögren, W. R. Salaneck, S. Stafström, J. Chem. Phys., 97, (1992) 137.
80. M. Deleuze, J. Delhalle, B. T. Pickup, S. Svensson, J. Am. Chem. Soc., 116, (1994) 10715.
81. M. Takahashi, K. Otsuka, Y. Udagawa, Chem. Phys., 227, (1998) 375.
82. M. Takahashi, R. Ogino, Y. Udagawa, Chem. Phys. Lett., 288, (1998) 821.
83. S. F. Zhang, X. G. Ren, G. L. Su, C. G. Ning, H. Zhou, B. Li, G. O. Li, and J. K. Deng, Chem. Phys., 327, (2006) 269.
84. J. H. D. Eland, Int. J. Mass. Spectrom. IonPhys., 2, (1969) 471.
85. I. D. Clark and D. C. Frost, J. Amer. Chem. Soc., 89, (1967) 244.
86. J. A. Pople, Trans. Faraday Soc., 49, (1953) 1375.
87. M. J. S. Dewar and G. J. Gleicher, J. Amer. Chem. Soc., 87, (1965) 685.
88. F. B. Billingsley, II, and J. E. Bloor, Theor. Chim. Acta, 11, (1968) 325.
89. M. J. S. Dewar and A. J. Harget, Proc. Roy. Soc. Ser. A, 315, (1970) 443.

90. N. O. Lipari and C. B. Duke, J. Chem. Phys., 63, (1975) 1748.

91. W. K. Ford, C. B. Duke, and W. R. Salaneck, J. Chem. Phys., 77, (1982) 5030.

92. W. K. Ford, C. B. Duke, and A. Paton, J. Chem. Phys., 77, (1982) 4564.

93. R. W. Bigelow, J. Chem. Phys., 66, (1977) 4241.

94. R. W. Bigelow, J. Chem. Phys., 67, (1977) 4498.

95. W. K. Ford, C. B. Duke, and A. Paton, J. Chem. Phys., 78, (1983) 4734.

96. E. M. Conwell, C. B. Duke, A. Paton, and S. Jeyadev, J. Chem. Phys., 88, (1988) 3331.

97. G. Nicolas and Ph. Durand, J. Chem. Phys., 70, (1979) 2020.

98. J. L. Bredas, R. R. Chance, R. H. Baughman, and R. Silbey, J. Chem. Phys. 76, (1982) 3673.

99. J. L. Bredas, R. R. Chance, R. Silbey, G. Nicolas, and Ph. Durand, J. Chem. Phys. 77, (1982) 371.

100. S.P. Kowalczyk, S. Stafström, J. L. Brédas, W. R. Salaneck, J. L. Jordan-Sweet, Phys. Rev. B, 41, (1990) 1645.

101. J. L. Bredas and G. B. Street, J. Chem. Phys., 82, (1985) 3284.

102. M. Ehara, Y. Ohtsuka, H. Nakatsuji, M. Takahashi, and Y. Udagawa, J. Chem. Phys., 122, (2005) 234319.

103. A. B. Trofimov, I. L. Zaitseva, T. E. Moskovskaya, and N. M. Vitkovskaya Chemistry of Heterocyclic Compounds, 44, (2008) 1101.

104. S. D. Worley, Chem. Rev., 71, (1971) 295.

105. T. Shida, Y. Nosaka, and T. Kato, J. Phys. Chem., 82, (1978) 695.

106. a) E, Fermi. 2. Phys. 1928, 48, 73 b) Thomas, L. H. Proc. Cambridge Philos. 927,23,542.

107. P. Hohenberg, W. Kohn, Phys. Rev. B, 136, (1964) 864.

108. W. Kohn, L. J. Sham, Phys. Rev. A, 140, (1965) 1133.

109. A. D. Becke, Phys. Rev. A, 38, (1988) 3098.

110. J. P. Perdew, Y. Wang, Phys. Rev. B, 33, (1986) 8800.

111. J. P. Perdew, Phys. Rev. B, 33, (1986) 8822.

112. C. Lee, W. Yang, R. G. Parr, Phys. Rev. B, 37, (1988) 785.

113. J. P. Perdew, R. G. Parr, M. Levy, J. L. Balduz, Jr., Phys. Rev. Lett., 49, (1982) 1691.

114. T. Ziegler, Chem. Rev., 91, (1991) 651.

115. S. B. Trickey, Phys. Rev. Lett., 56, (1986) 881.

116. R. Stowasser, R. Hoffman, J. Am. Chem. Soc., 121, (1999) 3414.

117. P. Politzer, F. Abu-Awwad, Theor. Chem. Acc., 99, (1998) 83.

118. U. Salzner, J. B. Lagowski, P. G. Pickup and R. A. Poirier, J. Phys. Chem. A, 102, (1998) 2572.

119. E. Runge, E. K. U. Gross, Phys. Rev. Lett., 52, (1984) 997.

120. A. Dreuw, M. Head-Gordon, Chem. Rev., 105, (2005) 4009.

121. S. Grimme, M. Parac, Chem. Phys., 292, (2003) 11.

122. S. Hirata, M. Head-Gordon, Chem. Phys. Lett., 302, (1999) 375.

123. M. J. Frisch, G. W. Trucks, H. B. Schlegel, G. E. Scuseria, M. A. Robb, J. R. Cheeseman, J. A. Montgomery, Jr., T. Vreven, K. N. Kudin, J. C. Burant, J. M. Millam, S. S. Iyengar, J. Tomasi, V. Barone, B. Mennucci, M. Cossi, G. Scalmani, N. Rega, G. A. Petersson, H. Nakatsuji, M. Hada, M. Ehara, K. Toyota, R. Fukuda, J. Hasegawa, M. Ishida, T. Nakajima, Y. Honda, O. Kitao, H. Nakai, M. Klene, X. Li, J. E. Knox, H. P. Hratchian, J. B. Cross, V. Bakken, C. Adamo, J. Jaramillo, R. Gomperts, R. E. Stratmann, O. Yazyev, A. J. Austin, R. Cammi, C. Pomelli, J. W. Ochterski, P. Y. Ayala, K. Morokuma, G. A. Voth, P.

Salvador, J. J. Dannenberg, V. G. Zakrzewski, S. Dapprich, A.D. Daniels, M. C. Strain, O. Farkas, D. K. Malick, A. D. Rabuck, K. Raghavachari, J. B. Foresman, J. V. Ortiz, Q. Cui, A. G. Baboul, S. Clifford, J. Cioslowski, B. B. Stefanov, G. Liu, A. Liashenko, P. Piskorz, I. Komaromi, R. L. Martin, D. J. Fox, T. Keith, M. A. Al-Laham, C. Y. Peng, A. Nanayakkara, M. Challacombe, P. M. W. Gill, B. Johnson, W. Chen, M. W. Wong, C. Gonzales, J. A. Pople, Gaussian 03, revision D. 01; Gaussian, Inc.: Wallingford, CT, 2004.

124. A. D. Becke, J. Chem. Phys., 98, (1993) 5648.
125. W. J. Stevens, H. Basch, J. Krauss, J. Chem. Phys., 81, (1984) 6026.
126. W. J. Stevens, M. Krauss, H. Basch, P. G. Jasien, Can. J. Chem., 70, (1992) 612.
127. R. Pariser, J. Chem. Phys., 24, (1956) 250.
128. U. Salzner, J. Chem. Theor. Comput., 3, (2007) 219.
129. M. Cossi, R. Cammi, J. Tomasi, Chem. Phys. Lett. 255, (1996) 327.
130. G.R. Branton, D.C. Forest, T.Makita, Phil. Trans. Roy. Soc. Lond. A. 268 (1970), 77.
131. Potts, A. W.; Price, W. C., Proc. R. Soc. Lond. A, 326 (1972), 181.
132. S. Suzer, S. T. Lee, and D. A. Shirley, Phys. Rev. A 13, (1976) 1842.
133. R. I. Martin and D. A. Shirley, J. Chem. Phys. 64, (1976) 3685.